AGU ADVANCING EARTH AND SPACE SCIENCE

JGR Planets

RESEARCH ARTICLE
10.1029/2019JE006260

Key Points:
- Paleomagnetic measurements of carbonaceous chondrites can provide important constraints on outer solar system magnetic fields
- Our measurements on primitive CR chondrules show that they formed in a magnetic field ≤8 μT
- Such low fields suggest either spatial variations in the nebular magnetic field or incipient dissipation of the nebula by 3.7 Myr after CAIs

Correspondence to:
R. R. Fu,
rogerfu@fas.harvard.edu

Citation:
Fu, R. R., Kehayias, P., Weiss, B. P., Schrader, D. L., Bai, X.-N., & Simon, J. B. (2020). Weak magnetic fields in the outer solar nebula recorded in CR chondrites. *Journal of Geophysical Research: Planets*, *125*, e2019JE006260. https://doi.org/10.1029/2019JE006260

Received 29 OCT 2019
Accepted 31 MAR 2020
Accepted article online 30 APR 2020

Author Contributions:
Conceptualization: Benjamin P. Weiss, Devin L. Schrader
Formal analysis: Pauli Kehayias
Funding acquisition: Benjamin P. Weiss
Investigation: Pauli Kehayias
Methodology: Pauli Kehayias, Benjamin P. Weiss, Devin L. Schrader
Project administration: Benjamin P. Weiss
Software: Pauli Kehayias
Supervision: Benjamin P. Weiss
Validation: Benjamin P. Weiss
Writing – review & editing: Pauli Kehayias, Benjamin P. Weiss, Devin L. Schrader, Xue-Ning Bai, Jacob B. Simon

Weak Magnetic Fields in the Outer Solar Nebula Recorded in CR Chondrites

Roger R. Fu[1], Pauli Kehayias[1,2], Benjamin P. Weiss[3], Devin L. Schrader[4], Xue-Ning Bai[5], and Jacob B. Simon[6,7,8]

[1]Department of Earth and Planetary Sciences, Harvard University, Cambridge, MA, USA, [2]Sandia National Laboratories, Albuquerque, NM, USA, [3]Department of Earth Atmospheric, and Planetary Sciences, Massachusetts Institute of Technology, Cambridge, MA, USA, [4]Center for Meteorite Studies, School of Earth and Space Exploration, Arizona State University, Tempe, AZ, USA, [5]Institute for Advanced Study, Tsinghua University, Beijing, China, [6]Department of Physics and Astronomy, Iowa State University of Science and Technology, Ames, IA, USA, [7]JILA, University of Colorado Boulder and NIST, Boulder, CO, USA, [8]Department of Space Studies, Southwest Research Institute, Boulder, CO, USA

Abstract Theoretical investigations suggest that magnetic fields may have played an important role in driving rapid stellar accretion rates and efficient planet formation in protoplanetary disks. Experimental constraints on magnetic field strengths throughout the solar nebula can test the occurrence of magnetically driven disk accretion and the effect of magnetic fields on planetary accretion. Here we conduct paleomagnetic experiments on chondrule samples from primitive CR (Renazzo type) chondrites GRA 95229 and LAP 02342, which likely originated in the outer solar system between 3 and 7 AU approximately 3.7 million years after calcium aluminum-rich inclusion formation. By extracting and analyzing 18 chondrule subsamples that contain primary, igneous ferromagnetic minerals, we show that CR chondrules carry internally non-unidirectional magnetization that requires formation in a nebular magnetic field of $\leq 8.0 \pm 4.3$ μT (2σ). These weak magnetic fields may be due to the secular decay of nebular magnetic fields by 3.7 million years after calcium aluminum-rich inclusions, spatial heterogeneities in the nebular magnetic field, or a combination of both effects. The possible inferred existence of spatial variations in the nebular magnetic field would be consistent with a prominent role for disk magnetism in the formation of density structures leading to gaps and planet formation.

Plain Language Summary Stars and their planetary systems form from large, flattened structures composed of low-density gas and dust called protoplanetary disks. Two major unresolved questions regarding protoplanetary disks are the mechanisms that limit their lifetimes to a few million years and the mechanisms that create the first planets from dust particles. Turbulence in the gas caused by action of magnetic fields have been hypothesized as explanations for both of these processes. In our study, we measure the permanent magnetization of ~1 mm-sized inclusions from two meteorites called GRA 95229 and LAP 02342. These inclusions are believed to have formed ~3.7 Ma after the formation of the protoplanetary disk around the Sun and beyond about 3 astronomical units (AU) from the Sun (1 astronomical unit is the Earth-Sun distance equal to $\sim 150 \times 10^6$ km). We find that the inclusions formed in a magnetic field of ≤8 μT, a fraction of the surface magnetic field on Earth and lower than expected from previous measurements in the protoplanetary disk closer to the Sun. This potentially provides evidence for heterogeneities in the nebular gas, which may be the locations of planet formation or partial dissipation of the disk in 3.7 million years.

1. Introduction

Many fundamental questions regarding the mechanisms of planet formation and protoplanetary disk evolution remain unanswered. Collisions between solid aggregates larger than ~1 cm tend to yield disintegration instead of growth (e.g., Zsom et al., 2010). This well-documented barrier to planet formation has motivated the hypothesis that pressure bumps in the nebular gas efficiently concentrated mm- to cm-sized particles into self-gravitating clumps. In this scenario, self-gravity drives the accretion of particles into the first planetesimals, circumventing the need for individual particle-particle collisions to result in accretion [e.g., (Carrera et al., 2015; Chambers, 2010; Johansen et al., 2007; Johansen et al., 2015; Krapp et al., 2018; Zhu & Stone, 2014)]. At the same time, observed stellar accretion rates and disk lifetimes require highly efficient angular momentum transport, which is critical for the inward transport of disk material and is partially responsible for the ultimate depletion of the protoplanetary disk.

However, the ultimate origin of density concentrations and angular momentum transport in disks is poorly understood, with both magnetic and non-magnetic, hydrodynamic processes invoked in different regions of the disk (for review see Klahr et al., 2018). A central challenge of modeling the role of magnetic fields in disks has been the treatment of low ionization fractions in the disk gas, which results in the coexistence of multiple non-ideal magnetohydrodynamics (MHD) regimes where magnetic fields are not fully coupled to the gas. Recent studies have incorporated complex reaction networks to quantify the degree of gas ionization and explicitly compute all expected non-ideal MHD effects [e.g., (Bai & Stone, 2013; Kunz & Lesur, 2013; Simon, Bai, Armitage, et al., 2013; Simon, Bai, Stone, et al., 2013; Lesur et al., 2014; Simon et al., 2015)].

Some such disk models suggest that, once these non-ideal MHD effects are accounted for, magnetically driven self-organization may lead to local density enhancement (Béthune et al., 2017; Krapp et al., 2018). Such density enhancements, in turn, can facilitate planet formation if clumps of concentrated particles become sufficiently large and dense to be self-gravitating. Alternatively, the presence of a “snow line,” outside of which the presence of ice particles leads to a rapid change in the inward drift rate of particle, can also result in gap and ring formation (Hu et al., 2019). If such particle traps exist in real protoplanetary disks, they may be critical in the accretion of planetesimals and explain recent observations of gap and ring structures from the Atacama Large Millimeter Array (ALMA; (ALMA Partnership et al., 2015; Isella et al., 2016)).

With respect to the role of magnetism in angular momentum transport, simulations incorporating non-ideal MHD effects have begun to converge toward a paradigm where distinct magnetically driven processes operate in different parts of the protoplanetary disk. In the largely laminar midplane region within ~10 AU, known as the dead zone (Gammie, 1996), substantial transport may occur due to the Hall shear instability (see Kunz, 2008 for physical derivation), which amplifies the magnetic field strength (Bai, 2017; Béthune et al., 2017). In the surface regions of the inner disk, magnetized disk winds may be the primary mechanism of mass and angular momentum transport, while the magnetorotational instability may dominate the outer disk beyond ~10 AU (Bai, 2015; Simon, Bai, Armitage, et al., 2013). Although a physical explanation of these mechanisms is beyond the scope of this paper, review articles are available for the magnetorotational instability (Balbus & Hawley, 2000) and disk winds (Bai & Stone, 2013).

Despite the rapid progress in theoretical understanding, significant uncertainties remain in key aspects of MHD disk models. Some outcomes of numerical models depend on the choice of numerical parameters such as resolution and initial and boundary conditions (Bai, 2017; Ryan et al., 2017). Critical physical parameters including the net vertical magnetic field flux and the ionization level of the nebular gas remain poorly constrained (Bai, 2017; Bai & Stone, 2017; Béthune et al., 2017; Simon et al., 2018). Finally, recent MHD models diverge significantly regarding the degree and origin of spatial variations in magnetic field strength throughout the planet-forming region.

Therefore, observational and experimental constraints on the nature of protoplanetary disk magnetic fields are critical for evaluating the reliability of disk magnetism models and ultimately understanding the role of magnetism on planetary system formation. Polarimetry observations, which are the telescopic measurement of alignment in non-spherical dust grain populations, may reveal the geometry and approximate strength of magnetic fields in distant protoplanetary disks (Alves et al., 2018; Crutcher, 2012; Kataoka et al., 2015; Li et al., 2016; Stephens et al., 2014; Vlemmings et al., 2019). However, such techniques cannot currently probe the dense, planet-forming regions in the disk interior with high accuracy, while the mechanism of grain polarization is poorly understood, leading to uncertainties in the interpretations of the observed magnetic field geometry (Andersson et al., 2015; Ohashi et al., 2018; Stephens et al., 2017).

Alternatively, paleomagnetic measurements on meteoritic materials can quantify magnetic field strengths in the early solar system and currently represent the only observational means to study magnetic fields in the protoplanetary disk midplane where planet formation occurs. Igneous components of chondritic meteorites, such as chondrules and calcium aluminum-rich inclusions (CAIs), underwent heating and cooling in the presence of the nebular gas and therefore may have acquired a thermoremanent magnetization (TRM) that records information about ancient magnetic field strengths.

Paleomagnetic studies seek to characterize nebular magnetic fields by isolating the magnetic signal from such igneous components. A previous paleomagnetic study of the Semarkona LL3.0 chondrite targeted dusty olivine-rich chondrules, which contain primary ferromagnetic iron particles formed from exsolution during igneous reduction of fayalitic olivine (Fu, Weiss, et al., 2014). The authors concluded that, assuming that the chondrule formation mechanism did not significantly enhance background field levels, magnetic fields of ~50 μT existed in the inner solar nebula at ~2 Myr after the formation of CAIs, which is approximately the formation time of the solar system. We will return to the implications of this magnetic field intensity for disk magnetism in section 4.

In addition to providing information about the magnetization state of nebular gas, paleomagnetic measurements targeting chondrules can constrain how chondrules formed, a long-standing unsolved problem in planetary science. TRM acquisition in a spinning object requires a stable rotation axis orientation with respect to the magnetic field; therefore, the existence of TRM in individual chondrules places an upper bound on the interchondrule collision frequency (Fu et al., 2018; Schrader, Fu, et al., 2018). Finally, the strength of magnetic fields during the cooling phase of chondrule formation is potentially informative regarding the formation mechanism itself (Fu et al., 2018; Mai et al., 2018; Shu et al., 1996).

A recent study of three rapidly cooled angrite achondrites, which is a group of rapidly cooled basaltic meteorites, showed that nebular magnetic fields in the angrite formation region were weaker than ~0.6 μT at 3.8 Myr after CAI formation (Wang et al., 2017). These intensities are much weaker than those inferred from Semarkona and may represent decay in the gas density of the solar nebula by 3.8 Myr after CAI formation. Alternatively, angrites may have formed in regions of the nebula with very low magnetic field strength where the net vertical magnetic field is not strongly amplified due to MHD processes or where processes redistribute the net vertical flux [see section 4; (Bai, 2017; Béthune et al., 2017)]. However, the latter alternative is unlikely because MHD simulations suggest that only a small volume of the disk midplane has magnetic fields weaker than 0.6 μT (see supplementary section 1.2 of Wang et al., 2017 and Figures 4, 16, and 20 of Béthune et al., 2017).

The recovery of magnetic field records from other chondrite groups may provide constraints on disk dynamics at other times and locations. The observed diversity in multiple isotopic systems suggests that carbonaceous chondrites originated from a distinct chemical reservoir compared to ordinary chondrites, possibly beyond the orbit of Jupiter or another significant gap in the solar nebula (Kruijer et al., 2017; Sutton et al., 2017). Paleomagnetic studies of nebular magnetic fields based on carbonaceous chondrites have been limited by the rarity of unaltered ferromagnetic minerals (Fu et al., 2018). Recent studies of both CV and CM chondrites provide evidence of ancient magnetic fields with 2–60 μT intensity (Carporzen et al., 2011; Cournede et al., 2015). However, I-Xe isotopic ages from CV chondrites indicate post-nebular formation of the main ferromagnetic minerals, suggesting that the recorded field was of parent body dynamo origin. Meanwhile, thermal modeling of the CM chondrite parent body argues that the formation of ferromagnetic minerals likely preceded any core dynamo, suggesting that these meteorites record a nebular magnetic field (Bryson et al., 2019). However, the intensity of the recorded field remains highly uncertain due to the non-thermal origin of the remanent magnetization.

In this work, we present paleomagnetic measurements on isolated chondrules from CR (Renazzo type) carbonaceous chondrites, which have an average crystallization age of $3.7^{+0.3}_{-0.2}$ Myr after CAIs and may have originated from beyond the orbit of Jupiter (Kruijer et al., 2017; Schrader et al., 2017). To minimize the effect of overprinting mechanisms such as aqueous alteration and impact shock, we limit our samples to igneous iron sulfide-bearing chondrule rims and FeNi metal-bearing chondrules from the primitive CR chondrites GRA 95229 and LAP 02342, respectively. We find non-unidirectional magnetizations within single chondrules of both meteorites, indicating that magnetic fields were weaker than ~8 μT in the CR chondrule formation environment. We then discuss the implications of this and other chondrule-derived paleointensities on our understanding of protoplanetary disk dynamics.

2. Materials and Methods

We chose the CR2 chondrites GRA 95229 and LAP 02342 for this study due to the low degree of postaccretional thermal metamorphism and aqueous alteration (Schrader et al., 2015). We first studied bulk samples, which consist of matrix, chondrule material, and sometimes fusion crust, to characterize post-accretion

10.1029/2019JE006260

Table 1
Summary of Samples, Experiments, and Laboratory Apparatus Used

Samples	Experiment	Instrument
Bulk fusion crust and interior	AF demagnetization of NRM	2G SRM
GRA 95229 sulfide-rich chondrule rim	AF demagnetization of NRM	QDM; RAPID system
	ARM acquisition	QDM; RAPID system
	Backfield IRM acquisition	QDM; ASC IM-10-30 Impulse magnetizer
	Thermal demagnetization of IRM (Lowrie test)	QDM; ASC TD48SC oven
	Backscatter electron (BSE) mapping	JEOL 7900 SEM
LAP 02342 chondrule samples	AF demagnetization of NRM	SQUID microscope; RAPID system
	Thermal demagnetization of NRM	SQUID microscope; ASC TD48SC oven
	ARM acquisition	SQUID microscope; RAPID system
	Backscatter electron (BSE) mapping	JEOL 7900 SEM

Note. RAPID system (Rock and Paleomagnetism Instrument Development) refers to the use of the AF and ARM coils supplied with the 2G SRM.

overprints (Tables 1 and 2). We then measured subsamples of individual chondrules to recover any record of nebular magnetic fields (Table 3). Because both meteorites have undergone significant aqueous alteration, especially in the fine-grained matrix, we focused our chondrule analyses on sub-regions that retain two classes of primary, unaltered ferromagnetic phases: Fe sulfide-rich chondrule rims in GRA 95229 and unaltered FeNi grains in the chondrule interiors of LAP 02342.

With respect to sulfide-rich rims in GRA 95229, previous compositional and textural data have shown that GRA 95229 sulfide rims are primary igneous phases formed during late stage cooling between 600 and 400 °C (Schrader et al., 2015; Singerling & Brearley, 2018). In the case of chondrule interior FeNi grains in LAP 02342, the low frequency (24–30%) of exsolution textures observed using scanning electron microscope (SEM) imaging indicates that these grains are likely in the form of martensite (α_2-FeNi) and provide evidence for metamorphism well below ~200 °C (Briani et al., 2013; Kimura et al., 2002). Our SEM analyses of metal grains in our paleomagnetic samples, performed using a JEOL 7900 SEM at the Harvard Center for Nanoscale Systems (CNS), confirm the lack of chemical alteration and exsolution, especially plessite exsolution which may compromise the primary paleomagnetic record (Figures 1c–1e). Furthermore, the heterogeneous distribution of exsolved metal phases among sub-regions of the meteorite may indicate that the associated heating events occurred before the accretion of chondrules onto the CR parent body (Briani et al., 2013). In this scenario, any partial thermoremanent magnetization imparted on the chondrules would still record the nebular magnetic field, although not necessarily during a chondrule formation event.

We extracted both bulk and chondrule specimens from parent samples GRA 95229,115 and LAP 02342,41 obtained from the the National Aeronautics and Space Administration (NASA) Antarctic Meteorite Collection at Johnson Space Center. Both classes of samples have typical dimensions of 100–700 μm (Figure 1). To obtain well-oriented samples of such size with precisely defined boundaries, we first cut the GRA 95229 and LAP 02342 parent pieces into two to four slices of 100–150 μm thickness using a Well diamond wire saw. Each slice was mounted using cyanoacrylate to a non-magnetic GE 124 fused quartz disk, lightly polished using 1 μm alumina grit, and imaged using a petrographic microscope to identify regions of interest.

We then used non-magnetic tungsten carbide dental tools mounted on an Electro Scientific Industries Inc. Micromill, which has lateral reproducibility of ~5 μm, to cut grooves around the desired regions, thereby isolating them from the surrounding material. We detached the isolated samples using acetone and mounted them to separate GE 124 fused quartz disks with cyanoacrylate. Because all samples had a flat, saw cut surface, we were able to recover their three-dimensional orientations to better than 3° accuracy based on in situ petrographic microscope images (see above). Samples subjected to alternating field (AF) demagnetization remained on the GE 124 disks during the sequence. Following Fu et al. (2017), samples subjected to thermal demagnetization were placed in micromilled wells in Corning® Eagle XG® glass substrate and immobilized with high purity quartz powder.

Table 2
Summary of NRM Directions Observed in Bulk Samples, Including Fusion Crust ("F.C.") Samples

Name	Distance to fusion crust (mm)	Component	Range (mT)	*N*	Dec., Inc. (°)	MAD (°)	Included in fusion crust mean
GM1	0	LC	0–9.5	18	13.4, 13.8	20.8	
		HC	9.5–120	86	123.2, −24.8	13.5	Yes
GM2	0	LC	0–9	17	34.1, 40.6	13.4	
		HC	9–120	87	134.5, −13.2	19.4	Yes
GM3	1.0	None					
GM4	1.0	None					
GM5	0	LC	0–11	21	26.6, 6.9	13.3	
		HC	11–92	81	126.0, −33.7	9.5	Yes
GM6	0	LC	0–11	21	341.0, 52.0	33.5	
		HC	11–58	79	123.4, −33.5	18.2	Yes
F.C. Mean (LC)				4	16.4, 29.5	33.5 (α_{95})	
F.C. Mean (HC)				4	127.0, −26.4	12.4 (α_{95})	

Name	Distance to fusion crust (mm)	Component	Range (mT)	*N*	Direction (°)	MAD (°)	
LM1	0	HC	0–75	13	301.5, −2.7	18.5	Yes
LM2	0.2	LC	0–65	12	71.6, −16.3	13.4	Yes
		HC	65–125	7	170.6, 1.2	17.8	
LM3	0.2	LC	0–32.5	7	127.4, −62.8	13.9	
LM4	0.6	None					
LM5	1.3	None					
LM6	0	HC	0–85	14	35.0, −38.9	11.8	Yes
LM7	0	HC	22.5–95	11	313.9, −33.3	19.8	Yes
LM8	0.3	HC	0–75	11	45.9, −11.0	21.9	
LM9	0.3	HC	0–37.5	8	62.1, −19.9	9.6	
LM10	0.8	None					
LM11	0	HC	32.5–135	13	26.6, −58.6	16.4	Yes
LM12	0.7	LC	0–65	11	19.6, −37.0	13.8	Yes
		HC	65–142.5	10	128.6, 56.2	23.6	
LM13	5.1	None					
LM14	5.4	None					
LM15	6.3	HC	17.5–47.5	7	104.3, 7.0	11.3	
LM16	4.4	None					
LM17	4.5	None					
F.C. Mean				6	7.1, −42.0	45.0 (α_{95})	

Using these techniques, we extracted four fusion crust-bearing samples from GRA 95229 along with two samples ~1 mm from the fusion crust (Figure 1a and Table 2). For LAP 02342, we measured 17 bulk samples, four of which are fusion crust bearing. An additional six samples were from within 1.0 mm of the fusion crust surface, while the remaining samples were from the deeper interior (Figure 1b). To measure the magnetization of these bulk samples, we used 2G Enterprises model 755 superconducting rock magnetometers at the Massachusetts Institute of Technology (MIT) and Harvard Paleomagnetics Laboratories. We subjected all bulk samples to three-axis AF demagnetization until the remanent magnetization direction became unstable (≤142.5 mT). For each demagnetization step above 50 mT, we measured the sample magnetization after AF application in each of three mutually orthogonal directions to detect and correct for gyroremanent magnetization (Stephenson, 1993). We find no patterns in the resulting scatter of magnetization directions attributable to gyroremanent magnetization and compute the simple vector average of magnetizations measured at the same AF level to generate the final demagnetization sequence.

After testing for the lack of terrestrial remagnetization using the bulk samples (see section 3), we extracted and analyzed subsamples of individual chondrules to recover any records of nebular magnetic fields. We used the techniques described above to extract a total of 7 Fe sulfide-rich samples from a single, ~2 mm diameter chondrule from GRA 95229 land 11 subsamples from four separate chondrules from LAP 02342 (Figures 1a and 1b). All chondrule subsamples were located at least 3 mm from the nearest fusion crust. As with bulk specimens, chondrule subsamples were mutually oriented with ≤3° accuracy.

Table 3
Summary of NRM Component Directions Observed in Chondrule Samples

Name	Mass (mg)	Component	Range (mT or °C)	*N*	Dec., Inc. (°)	MAD (°)	Forced direction (°)	Forced MAD (°)	Forced difference (DANG, °)
G1a	0.0013	None							
G1b	0.0025	LC	15–82 mT	5	47.1, −16.6	18.4			
		HC	82–202 mT	3	204.3, −1.3	12.4	216.8, 3.9	9.2	13.5
G1c	0.0025	LC	0–15 mT	4	251.7, 18.1	15.2			
		HC	15–82 mT	5	67.6, −42.1	14	104.5, −27.7	16.6	33.2
G1d	0.0017	None							
G1e	0.0046	None							
G1f	0.0091	HC	25–50 mT	6	54.2, 23.0	23.4	36.3, −2.8	15.2	31.2
G1g	0.0075	HC	15–40 mT	3	344.8, −12.6	15.1	341.4, −36.9	18.4	24.5

Name	Mass (~~mg~~)	Component	Range (mT or °C)	*N*	Direction (°)	MAD (°)	Forced direction (°)	Forced MAD (°)	Forced difference (°)
L1a	0.094	None							
L1b	0.21	LC	NRM to 20 mT	4	182.6, −0.1	9.4			
		HC	15–60 mT	5	74.2, 2.0	14.8	78.9, 10.7	19.9	9.9
L1c	0.86	HC	NRM to 50 mT	8	167.4, −7.8	14.6	164.8, −0.8	26.1	7.5
L2a	0.20	None							
L2b	0.10	None							
L3a	0.036	None							
L3b	0.082	None							
L3c	0.032	None							
L4a	0.11	None							
L4b	0.097	HC	146–636 °C	6	141.5, 38.6	10.3	166.7, 44.7	26.3	19.7
L4c	0.097	HC	212–553 °C	4	228.4, 29.3	13.4	242.6, 31.6	31.5	12.4

Notes. Sample names that begin with "G" and "L" indicate GRA 95229 and LAP 02342, respectively. Directions and maximum angular deviation (MAD) were computed using principal component analysis making no assumption about trending toward the origin (Columns 6 and 7) and assuming that the component passes through the origin (Columns 8 and 9). The difference between these two computed directions is given in Column 10. In cases where data from multiple adjacent AF steps have been averaged, the coercivity given in the table is the weighted mean AF level of the averaged measurements. Chondrule subsample masses were estimated from the sample volume and an assumed density of 3,200 kg m^{-3}.

The weak natural magnetic moments of chondrule samples (3×10^{-13} to 4×10^{-11} Am^2) precluded their accurate measurement using the traditional 2G Enterprises superconducting rock magnetometer. We therefore used two different high-sensitivity magnetic imaging devices to map the magnetic field over each sample and quantitatively invert for the net magnetization (Table 1). The sulfide rim samples from GRA 95229 have typical dimensions between 100 and 150 μm (Figure 1), which is suitable for measurement on the Harvard quantum diamond microscope (QDM) with its 2.2 × 1.4 mm field of view (Glenn et al., 2017). We performed optically detected magnetic resonance (ODMR) experiments using the QDM to image the magnetic field in a plane ~20 μm over the surface of each sulfide sample with a spatial resolution of 4.68 μm per pixel. These ODMR measurements were made under a bias field of 0.9 mT, which was reversed multiple times during the course of measurement to eliminate any contribution from induced magnetization. We then upward continued all QDM maps by 50 μm to isolate the contribution of the dipole component and used a least squares fitting algorithm to compute the net magnetic moment (Lima & Weiss, 2009, 2016). To isolate individual components of natural remanent magnetization (NRM), we subjected all GRA 95229 chondrule samples to stepwise, three-axis AF demagnetization until the NRM became unstable (40–200 mT; Table 3). We repeated AF application and measurement up to four times at each AF step for higher demagnetization steps to mitigate noise.

Because sulfide-rich chondrule rims such as those occurring in GRA 95229 have not been studied magnetically, we conducted additional rock magnetic experiments consisting of isothermal remanent magnetization (IRM) backfield acquisition on samples G1b and G1c and stepwise thermal demagnetization in an ASC Scientific TD48SC oven of orthogonal IRMs acquired in saturating (0.8 T; oriented North) and 0.3 T (oriented East) fields, known as the Lowrie test (Lowrie, 1990), on sample G1c (Table 1). We recovered net sample moments for both rock magnetic samples using QDM imaging as described above. We did not attempt cryogenic cooling experiments to identify characteristic low-temperature transitions of magnetite and pyrrhotite

10.1029/2019JE006260

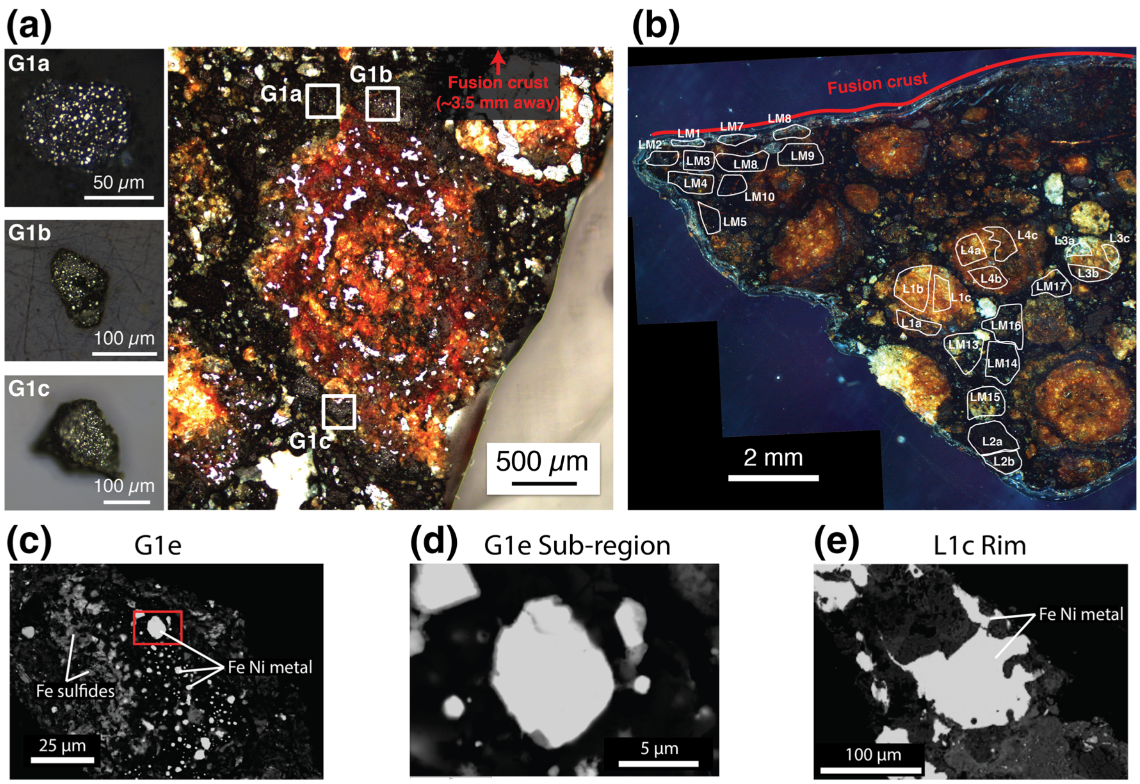

Figure 1. Optical photomicrographs of example (a) GRA 95229 and (b) LAP 02342 sections used in this study. Insets in panel (a) show sulfide-rich rim samples in the same orientation frame and were taken using reflected, plane-polarized light. Outlines in panel (b) denote the extraction locations of bulk (LM) and chondrule (L1–L4) samples. Large-scale maps were taken using reflected light mode with crossed polarizer. (c–e) Electron backscatter (BSE) maps of GRA 95229 chondrule rim sample G1e, an FeNi grain in G1e (red box in panel C), and an FeNi grain in the rim of chondrule L1 near sample L1c. Note the lack of exsolution features indicative of plessite formation.

because current instruments such as the Magnetic Properties Measurement System® (MPMS) are not sensitive enough to detect single chondrule samples.

For the larger, typically ≥500 μm chondrule samples from LAP 02342, we used the superconducting quantum interference device (SQUID) microscope in the MIT Paleomagnetism Laboratory to image magnetic fields over ~10 × 10 mm areas with 200 μm sample-sensor distance. We then upward continued the maps by 300–400 μm to isolate the dipole component of magnetic field and applied least squares fitting. The generally lower coercivity of LAP 02342 samples (Table 3) and the expectation of more multidomain behavior from FeNi metal implied that these samples are likely more susceptible to AF noise compared to those from GRA 95229 (Tikoo et al., 2012). As such, we subjected most LAP 02342 chondrule samples to stepwise thermal demagnetization up to 780 °C in a controlled H_2-CO_2 atmosphere with oxygen fugacity 2 log units below the iron-wüstite buffer (Table 3; Suavet et al., 2014). As a final step for chondrule samples from both meteorites, we performed anhysteretic remanent magnetization (ARM) acquisition experiments with a maximum AF of 290 mT and DC bias fields between 200 and 5 μT to quantify the magnetic field recording limit of each sample (Tikoo et al., 2012). All demagnetization data described here are available in the MagIC Database (Contribution #16701) and on the Harvard Dataverse (Fu et al., 2020). The latter repository also includes all raw QDM and superconducting quantum interference device microscope images.

3. Results

To identify components of NRM acquired after accretion onto the CR parent body, we performed principal components analysis on bulk material demagnetization sequences (Kirschvink, 1980). We isolated a low coercivity (<10 mT) and high coercivity (HC; 10–120 mT) component of magnetization in each of four fusion crust-bearing samples from GRA 95229 (Figures 2 and 3 and Table 2). In contrast, no coherent

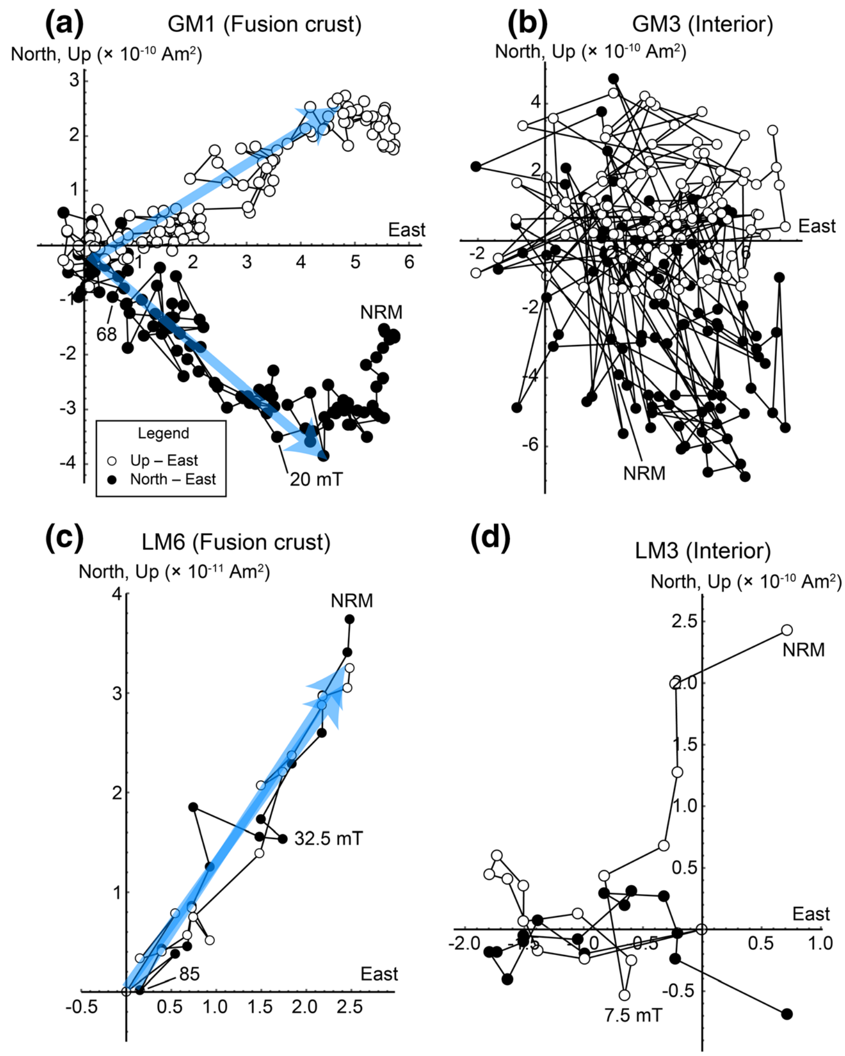

Figure 2. Orthogonal projection diagrams showing demagnetization behavior of bulk samples. AF demagnetization of (a) a fusion crust-bearing sample and (b) an interior sample from GRA 95229 reveal two distinct directions of magnetization associated with the fusion crust and no coherent magnetization direction in the interior. Similarly, (c) fusion crust-bearing samples from LAP 02342 carry single-component, unidirectional magnetizations, while (d) interior samples display low-coercivity, non-unidirectional magnetizations or no coherent magnetizations. Blue arrows highlight interpreted fusion crust remanence components. See Table 2 for tabulated component directions and properties from bulk samples. Open and closed symbols denote projections on up-east and north-east planes, respectively.

magnetization component is present in the two bulk samples extracted from 1.0 mm from the fusion crust. We therefore conclude that both magnetizations were likely acquired as the meteorite tumbled during atmospheric entry (Nagata, 1979a), although the softer coercivity range and larger scatter of the low coercivity component mayalso be a terrestrial VRM that preferentially affected the magnetic mineralogy of the fusion crust.

For LAP 02342, we identified a unidirectional HC component of magnetization in only the six samples extracted from within 0.5 mm of the fusion crust (Figures 2 and 3 and Table 2), again suggesting an atmospheric entry origin. Although low-coercivity components of magnetization were observed in deeper interior samples, they do not show coherent directions. In both meteorites, the absence of any unidirectional components of magnetization in interior bulk samples provides strong evidence that they have not been significantly remagnetized after arrival on Earth.

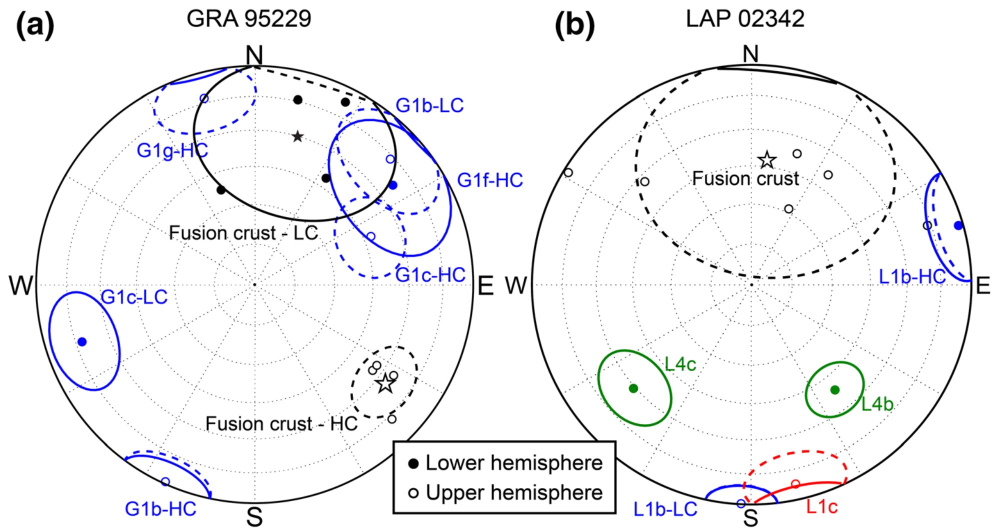

Figure 3. Equal area stereonets showing magnetization component directions in (a) sulfide-rich rim samples and fusion crust samples from GRA 95229 and (b) chondrule subsamples and fusion crust-bearing samples from LAP 02342. Each color represents data taken from distinct chondrules. Note the random orientations of the chondrule subsample directions. Open and close symbols denote projection on upper and lower hemispheres, respectively.

To check for the presence of secondary ferromagnetic minerals in our GRA 95229 chondrule samples, we conducted backfield IRM acquisition and thermal demagnetization of orthogonal IRM (Lowrie test) experiments (Figure 4 and Table 1). In particular, the presence of magnetite may indicate aqueous alteration of

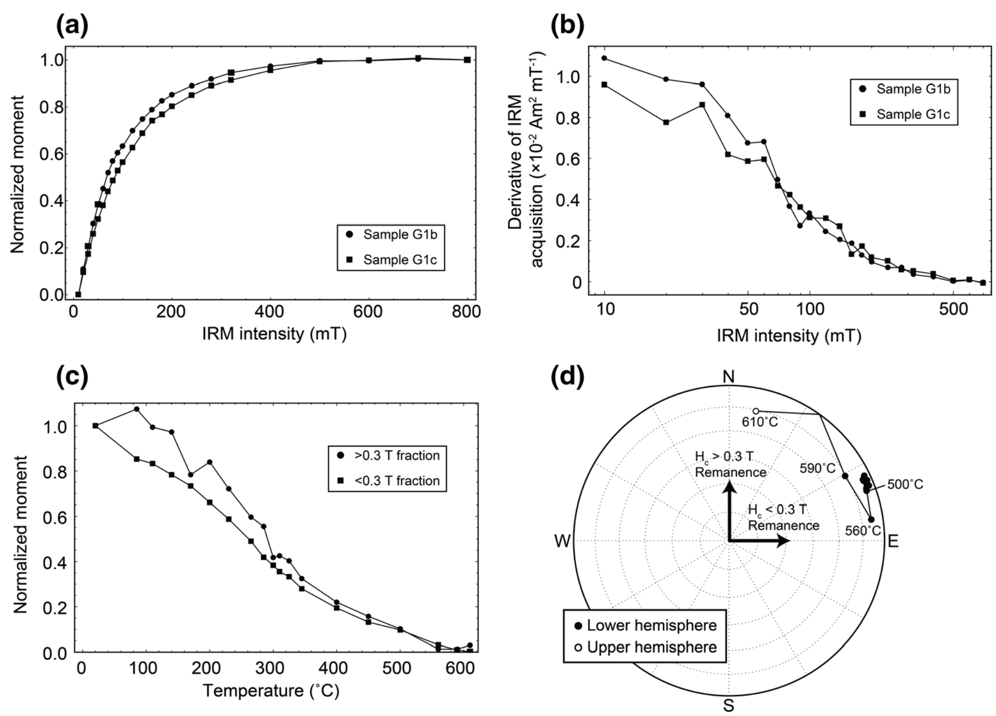

Figure 4. Rock magnetic analyses of Fe sulfide-rich chondrule rims from GRA 95229. (a) Backfield IRM acquisition sequence obtained after a saturating 1.4 T IRM in the opposing direction. (b) Derivatives of IRM acquisition sequence shown in panel (a). (c) Decay of magnetic moment in two coercivity ranges in sample G1c during thermal demagnetization after applying a saturating 0.8 T IRM in the north direction followed by a 0.3 T IRM in the east direction (Lowrie test). (d) Change in the moment direction during the Lowrie test sequence.

igneous Fe-bearing phases, while FeNi metal or Fe sulfides such as pyrrhotite are likely to date from chondrule formation (Davidson et al., 2019; Schrader et al., 2016). Based on these experiments, we make five observations relevant to the identity of the main ferromagnetic phase(s). First, maximum coercivities between 500 and 600 mT indicate the presence of at least one ferromagnetic carrier besides magnetite, which has a maximum coercivity of ~300 mT [Figure 4a; (Lowrie, 1990)]. Second, the 0.3 T eastward IRM imparted for the Lowrie test, which should include all potential magnetite-carried remanence, is not fully demagnetized until between 590 and 610 °C as indicated by the consistent northeasterly direction of magnetization (Figure 4d). These temperatures are above the magnetite Curie temperature of 580 °C, which demonstrates that at least one ferromagnetic phase other than magnetite carries the low coercivity fraction of IRM. Third, there is no significant rotation of the total remanence vector during the Lowrie test between room temperature and 590 °C, suggesting that the all types of ferromagnetic minerals in the sample contain grains with coercivity both >0.3 and <0.3 T. This provides evidence against the presence of magnetite due to its low coercivity. Fourth, the lack of any bimodality in the derivative of IRM acquisition supports the predominance of a single ferromagnetic mineral (Figures 4b and 4d). Finally, the thermal demagnetization curves of both coercivity ranges do not appear to show any concave-down behavior typical of Curie temperatures except a possible Curie point at ~290 °C.

Combining these observations, we conclude that remanence in GRA 95229 sulfide-rich rim samples is carried by a HC ferromagnetic phase that has a maximum unblocking temperature between 590 and 610 °C with a possible contribution from a second, HC ferromagnetic phase with Curie temperature ~290 °C. Neither of these phases can be magnetite due to its low unblocking temperature and coercivity. Instead, FeNi metal with 16–18 atomic percent (at%) Ni has an austenite start temperature consistent with the observed 590–610 °C loss of magnetization (Swartzendruber et al., 1991; Wasilewski, 1981). Published hysteresis experiments further confirm that our observed maximum coercivities are consistent with those of FeNi metal with 5% to ≥21 at% Ni (Tikoo et al., 2012; Wasilewski, 1981). Rapid cooling of an Fe-Ni-S system may result in metal grains with a range of compositions between 15 at% Ni in metastable cores and 30–50% in typical fully exsolved grains (Schrader & Lauretta, 2010). Based on these lines of evidence, we conclude that FeNi metal is the main ferromagnetic phase in GRA 95229 chondrule rim samples. In addition, sulfides such as hexagonal pyrrhotite (Fe_9S_{10}), which may be ferromagnetic at room temperature under some circumstances, may account for the possible second ferromagnetic phase with ~290 °C Curie temperature (Horng & Roberts, 2018). Our SEM imaging of chondrule samples from both CR chondrites further supports the identification of unexsolved FeNi and Fe sulfides as the main ferromagnetic phases (Figures 1c–1e).

AF demagnetization of GRA 95229 chondrule rims yielded identifiable components of NRM in four out of seven samples (Table 3). We observed a relatively high degree of scatter among successive measurements (Figure 5), which is likely due to a combination of multidomain response to AF demagnetization and statistical noise inherent to samples with very low moments (Berndt et al., 2016; Tikoo et al., 2012). We therefore performed vector averaging of between two and six adjacent AF steps at higher AF levels to reduce the uncertainty on the magnetization component direction. We identify trends in magnetization sequences as components of NRM if they contain at least three consecutive averaged demagnetization steps and have a maximum angular deviation (MAD) of less than 20°. We find that NRM components in all coercivity ranges exhibit directions that cannot be distinguished from a random distribution at 95% confidence [Figure 3; (Watson, 1956)].

Similarly, we observe identifiable NRM components in only 4 out of 11 LAP 02342 chondrule samples. The corresponding directions are again consistent with a random distribution both within and among single chondrules. Adopting different averaging windows for demagnetization steps or changing the MAD cutoff for identifying components leads to changes in the number of components and their directions (Table 3). However, the number of identified components does not alter the conclusions that, overall, a minority of chondrule samples have identifiable components and that these components display random directions. In fact, even the complete lack of identified components would result in the identical conclusion that these CR chondrules do not record a unidirectional magnetization.

To test whether these random distributions can be attributed to remanence anisotropy, we performed ARM acquisition experiments in strong DC fields (100–200 μT). The recovered magnetization directions in nine chondrule subsamples from both CR chondrites are within 25° of the laboratory bias field direction with

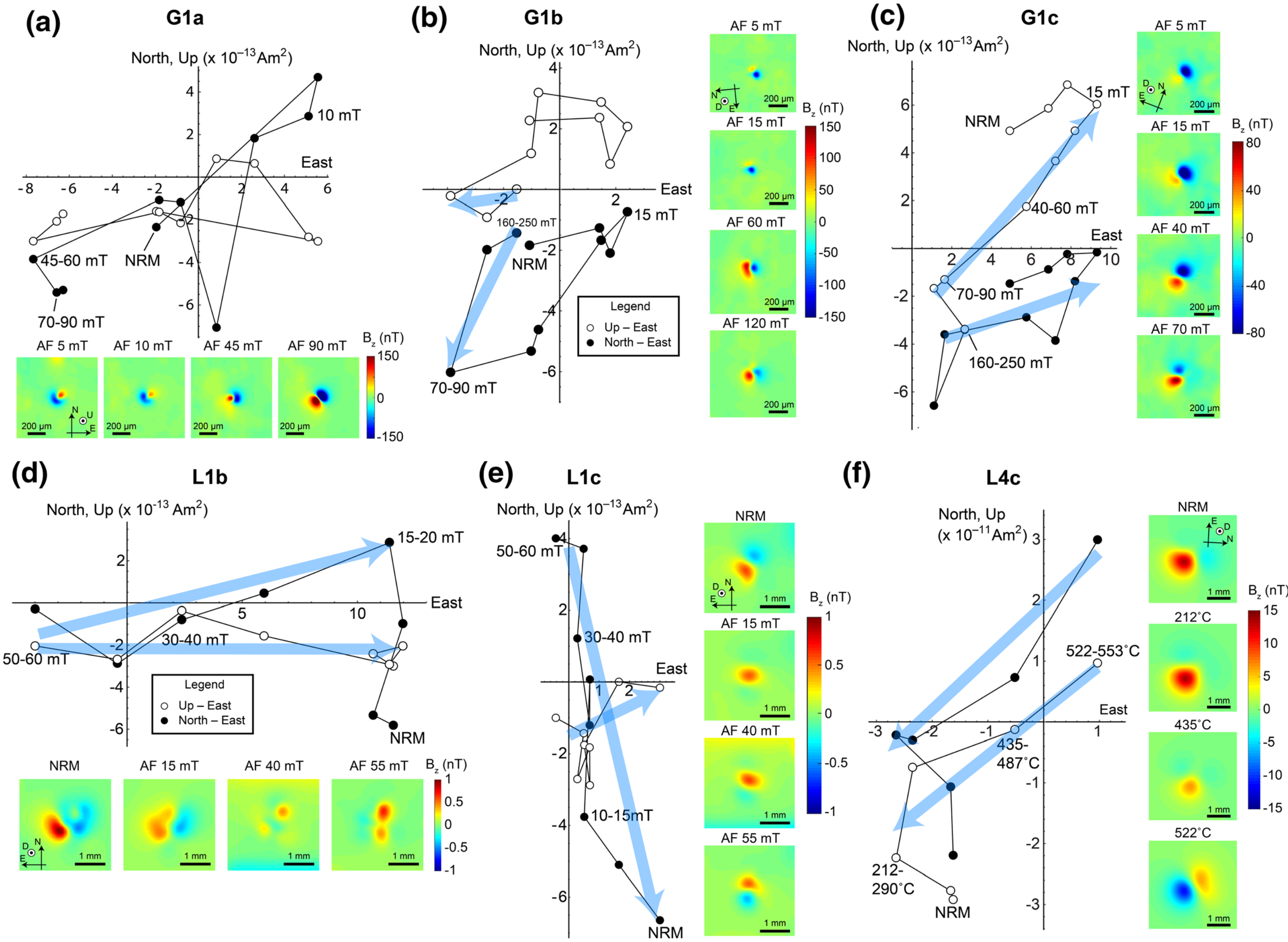

Figure 5. Demagnetization of NRM in GRA 95229 and LAP 02342. (a–c) Sulfide-rich chondrule rim sample G1a (a), G1b (b), and G1c (c) from GRA 95229 using the QDM. (d–f) Chondrule interior subsamples L1b (d), L1c (e), and L4c (f) from LAP 02342 using SQUID microscopy. Directions at higher demagnetization levels have been averaged to suppress noise. Diagrams in each panel are orthogonal projection diagrams showing evolution of the NRM during thermal and AF demagnetization, with open and closed symbols representing projections on north-east and up-east planes, respectively. Color inset maps in each panel are NRM field maps for selected demagnetization steps. Magnetic field maps shown here have been upward continued by 50 μm for GRA 95229 samples and by 400 μm for the larger LAP 02342 samples. These maps were then fitted to obtain the magnetization directions shown in the corresponding orthographic projections. Blue arrows represent the directions of the highest coercivity or temperature component of magnetization (if one was identified). Note that sample G1a carries no coherent NRM component. The coordinate system is given in the first magnetic field map of each panel where N, E, and D denote north, east, and down, respectively.

the exception of sulfide rim samples G1d (36°) and G1f (46°). Further, the mean ARM direction of even small 10–15 μT bias fields for multiple chondrule subsamples is within uncertainty (95% confidence interval; α_{95} = 25–32°) of the bias field direction (see below; Figure 6). In contrast, observed scatter among NRM components is in excess of 90°, indicating that the random NRM orientations cannot be explained by anisotropy.

The mechanistic origin of non-unidirectional NRM components is uncertain. Our chondrules are not brecciated, ruling out differential mechanical rotations of internal regions. Although the majority of visible ferromagnetic phases in our chondrule subsamples show no evidence for secondary minerals under optical and electron microscopy (see above and Samples and Methods; Figure 1), partial alteration of ferromagnetic phases on the CR parent body or in Antarctica may have resulted in chemical remanent magnetizations in scattered directions.

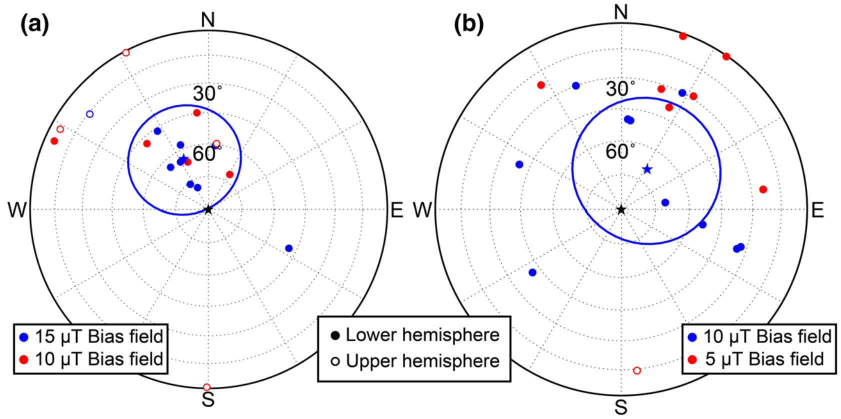

Figure 6. Results of ARM acquisition experiments to quantify the upper bound on the ambient magnetic field for (a) GRA 95229 and (b) LAP 02342 chondrules. Blue points, denoting ARM directions acquired in bias magnetic fields of 15 and 10 μT for GRA 95229 and LAP 02342, respectively, are the lowest bias field steps that show statistically non-random directions at 95% confidence that are consistent with the laboratory bias field direction. Red points, denoting the results of ARM acquisition in weaker fields of 10 and 5 μT, are indistinguishable from a random distribution at 95% confidence. Blue star and circle represent the mean and α_{95} uncertainties of non-random magnetizations acquired in stronger bias fields. Black star represents the ARM bias field direction. All ARMs were acquired in a 290 mT AC field.

Regardless of the origin of these scattered magnetizations, the absence of unidirectional magnetization within single chondrules in both CR chondrites contrasts with the NRM of dusty olivine-bearing Semarkona chondrules (Fu, Weiss, et al., 2014). This lack of coherent magnetization directions indicates that CR chondrule orientations were unstable relative to the background magnetic field or that magnetic fields during CR chondrule formation were too weak to impart a unidirectional TRM on the chondrules.

3.1. Chondrule Orientation During Cooling

We first consider the possibility that CR chondrules underwent rapid tumbling during cooling, resulting in the lack of coherent magnetizations. Adopting the commonly assumed minimum mass solar nebula (MMSN) conditions to describe gas density, the time needed for a chondrule's angular velocity to decrease by a factor *e* at 3 AU is approximately 10^3 hr (Fu & Weiss, 2012), which is longer than the likely cooling timescale of chondrules (see below). As such, an isolated chondrule is expected to retain a stable orientation relative to the background magnetic field and would acquire a remanent magnetization parallel to the spin axis if no interchondrule collisions occur.

We therefore estimate the frequency of interchondrule collisions for CR chondrules. The low Ni content of chondrule interior metal grains in LAP 02342 (~6–8 wt%; (Schrader et al., 2015)) corresponds to an expected Curie temperature of 760 °C and a martensite start temperature of ~650–700 °C (Reisener & Goldstein, 2003; Swartzendruber et al., 1991). Depending on a TRM or martensite transition origin for the NRM, these represent the temperature range at which magnetization acquisition initiated. Chondrule cooling rates around these temperatures are on the order 1–25 K h^{-1} (Wick & Jones, 2012). Meanwhile, inferred cooling rates at temperatures below the 325 °C Curie temperature of ferromagnetic monoclinic pyrrhotite are lower at 0.1–1 K h^{-1} (Schraderet al., 2018). Therefore, chondrules in both GRA 95229 and LAP 02342 likely acquired the bulk of their remanent magnetization over the course of order 100 to 1,000 hr.

Although these cooling timescales are longer than those at higher temperatures, the number of chondrule collisions at such a late cooling stage is also expected to be significantly lower. For the bow shock model of chondrule formation, the expected ambient density is less than ~4 times the background nebular density (Mai et al., 2018). Using a conservative estimate of 3 AU for the formation location (see below) and MMSN conditions with a dust to gas ratio of 25 (Boley et al., 2013), we estimate a chondrule number density of 0.006 m^{-3}. The expected number of interchondrule collisions then depends on the mean relative velocity, which remains highly uncertain with estimates between 0.001 and 1 m s^{-1} (Fu et al., 2018). Adopting this range of velocities and typical chondrule diameter and density of 1.0 mm and 3400 kg m^{-3}, we find that chondrules undergo an average of 7×10^{-6} to 7×10^{-3} collisions over the course of 100 hr in the bow shock model, implying that chondrule tumbling during remanence acquisition is highly unlikely.

For the impact jetting hypothesis of chondrule formation, Johnson et al. (2015) predicted 0.01 to 0.1 collisions per hour between 100 and 1,000 hr after chondrule heating, which may explain the lack of unidirectional magnetization in CR chondrites given an overall cooling timescale of 10–100 hr. However, these high collision frequencies appear inconsistent with the observed remanent magnetization in Semarkona chondrules and may be overestimated due to the assumption of an ejecta disk that expands only in the radial direction (Fu et al., 2018). We therefore conclude that CR chondrules likely underwent stable rotation relative to the background nebular magnetic field direction during cooling below the Curie temperature. However, if more refined modeling of impact-driven chondrule formation confirms the high estimated rates of interchondrule collisions, the lack of coherent magnetization in CR chondrules may support chondrule formation via this mechanism or another scenario predicting similarly high collision frequencies.

3.2. Chondrule Paleointensity

Second, we consider the possibility of weak ambient magnetic fields to explain the non-unidirectional chondrule NRM. Multidomain behavior and the limited number of ferromagnetic grains in chondrules may limit the ability of our samples to record a robust TRM even in the presence of a significant magnetic field (Berndt et al., 2016; Tikoo et al., 2012). We therefore performed ARM acquisition experiments on all seven GRA 95229 chondrule rim samples and two subsamples of the L1 chondrule from LAP 02342 in progressively weaker bias magnetic fields to quantify the minimum field intensity that can be recorded in these samples as a unidirectional magnetization.

We emphasize that the paleointensity upper bounds derived from this method do not assume that the observed non-unidirectional magnetizations in chondrule subsamples are of TRM origin and are not paleointensities derived from the components themselves. Instead, our ARM acquisition-based paleointensity quantifies the maximum field in which the chondrules would have acquired a unidirectional TRM, which is not in fact observed.

For these ARM acquisition experiments, we followed Fu, Lima, and Weiss (2014) and repeatedly applied AC magnetic fields with a peak amplitude of 290 mT and DC bias fields between 200 and 5 μT to multiple subsamples of single chondrules. Because measurement of a single AF demagnetization step for a single chondrule takes between and 1 and 2 hr on the current generation QDM, we found it time prohibitive to obtain AF demagnetization sequences for all imparted ARMs and instead use only the initial ARM direction. Because the AC field of the ARM (290 mT) is higher than observed NRM coercivities (≤250 mT), the acquired ARMs are expected to be single component; therefore, the initial ARM directions should be representative of the component direction if a full demagnetization sequence had been performed.

We consider a certain bias field as recordable if the repeat ARM directions from at least two samples are unidirectional (i.e., inconsistent with random directions) at 95% confidence. This method of quantifying the sample recording limit is based on the reasoning that the identification of a chondrule TRM in our NRM demagnetization sequences relies on the observation of unidirectional magnetizations in chondrule subsamples. If at least two subsamples of a single chondrule are capable of acquiring unidirectional ARMs in a given bias field, then we would expect that these subsamples should have acquired unidirectional NRM components during cooling in an ancient nebular magnetic field of similar strength. The absence of such unidirectional components would then suggest that nebular magnetic fields were weaker than the given ARM bias field.

We found that GRA 95229 subsamples G1b, G1f, and G1g acquired non-random magnetizations at 95% confidence consistent with the bias field direction during ARM acquisition in a 15 μT bias field [Figure 6; (Watson, 1956)] but acquired randomly oriented ARMs in a 10 μT bias field. For the L1b and L1c chondrule subsamples from LAP 02342, we recovered unidirectional and randomly oriented magnetizations after ARM acquisition in 10 and 5.0 μT bias fields, respectively. Reported values for the TRM to ARM efficiency (*f*) for FeNi metal-dominated samples are 0.91 (Lappe et al., 2013), 0.94 (Hoffman et al., 1979), 1.27 (Morden, 1992), 1.3 (Nagata, 1979b; Stephenson & Collinson, 1974), and 1.6 (Stephenson et al., 1976), yielding a mean value of 1.22 ± 0.52 (2σ). This implies that the GRA 95229 and LAP 02342 chondrule samples cooled in magnetic fields with effective strength of $\leq 8.1 \pm 5.4$ and 4.0 ± 2.2 μT, respectively. These calibration factors still apply in the scenario that remanence acquisition in the chondrules is due to martensite transition since several of the calibration experiments listed above were performed on lunar samples with typically >5 wt% Ni, which would undergo the same transition.

Finally, due to the likely rotation of chondrules (Fu et al., 2018; Fu, Weiss, et al., 2014), the true strength of the magnetic field during chondrule cooling was statistically a factor of 2 stronger than that recorded by individual chondrules. We therefore conclude that chondrules from the GRA 95229 and LAP 02342 CR chondrules cooled in magnetic fields weaker than 16.2 ± 10.8 and 8.0 ± 4.3 μT, respectively. Due to the potential for ARM noise to impart spurious magnetization on the sample (Tikoo et al., 2012), our weak-field ARMs likely exhibit greater scatter than TRMs under equivalent bias fields, implying that our experiments are likely overestimating the true TRM recording limits of the chondrules. As such, our ARM-derived paleointensities represent a generous upper bound on the field strength during chondrule cooling.

Given the expectation that the chondrules would have quickly reached internal thermal equilibrium during the cooling process, the non-unidirectional nature of the HC and HT magnetization components implies that they do not have a TRM origin. Similar non-unidirectional magnetizations have been reported previously in the Bensour and Semarkona LL chondrites, although in the latter they are only observed in non--dusty olivine-bearing chondrules (Fu, Weiss, et al., 2014; Gattacceca et al., 2003). The origin of such magnetizations is currently unknown, with spontaneous magnetization acquired during crystallographic growth, especially of tetrataenite, and brecciation following remanence acquisition (for Bensour) identified as possible explanations. The CR chondrites studied here were not heated to sufficient temperature to permit tetrataenite ordering [~200 °C; (Yang et al., 1997)]. However, the formation of small amounts of Fe oxides due to parent body alteration or on Earth may have led to the observed non-unidirectional magnetizations.

For completeness, we compute the ARM-normalized paleointensities of selected chondrule subsamples. In this technique, widely used for meteorites and other samples that are difficult to process with heating protocols (e.g., Weiss & Tikoo, 2014), the ancient magnetic field strength is estimated by computing the ratio of observed NRM component strength to an ARM acquired in a known laboratory field and multiplying this ratio with the laboratory bias field and a calibration constant (see above) that accounts for the mechanism of remanence acquisition. We evaluate ARM-normalized paleointensities using the identified component and the ARM acquired in a 25 μT bias field, resulting in 28 ± 12 μT for the four GRA 95229 chondrule subsamples with fitted components and 4.6 ± 1.2 μT for LAP 02342 chondrule subsamples L1b and L1c. The discrepancy between these values may be due to differences in the magnetic field environment where the magnetizations were acquired (e.g., Earth vs. parent body field) or different acquisition mechanisms. Because these magnetizations are not of TRM origin and their acquisition times are unknown, the implications of these ARM paleointensities remain unclear.

4. Discussion

Our observations of the NRM recorded in chondrules from CR chondrites GRA 95229 and LAP 02342 reveal no unidirectional components of magnetization, suggesting cooling in ambient magnetic fields weaker than ~8 μT. This field strength constraint can be applied to the solar nebula if we can establish that the nebular gas was still present at the time of CR chondrule formation and that the chondrule formation process did not strongly alter background nebula magnetic field levels.

Long- and short-lived radioisotope systems indicate that CR chondrules formed $3.7^{+0.3}_{-0.2}$ Myr after CAI formation (Budde et al., 2018; Schrader et al., 2017). This age is close to the ~3.8 Myr after CAIs age of angrites that recorded no significant magnetic field, likely due to gas depletion in the angrite formation region (Wang et al., 2017). However, the matrix of CR chondrules contains abundant <<1 μm-scale grains, which would be ejected from a gas-poor solar system in $<<10^5$ years due to radiation pressure and the Poynting-Robertson effect (Burns et al., 1979; de Pater & Lissauer, 2010; Kimura et al., 2002). Therefore, the nebular gas was likely still present and optically thick at peak solar radiation wavelengths at the time of CR chondrite accretion (Schrader, Nagashima, et al., 2018). Further, CR matrix grains are much finer and have more homogeneous thermal histories compared to the impact-produced matrices of CH and CB chondrites (Garvie et al., 2017). This implies that the CR matrix is not the product of late inter-planetesimal collisions, which

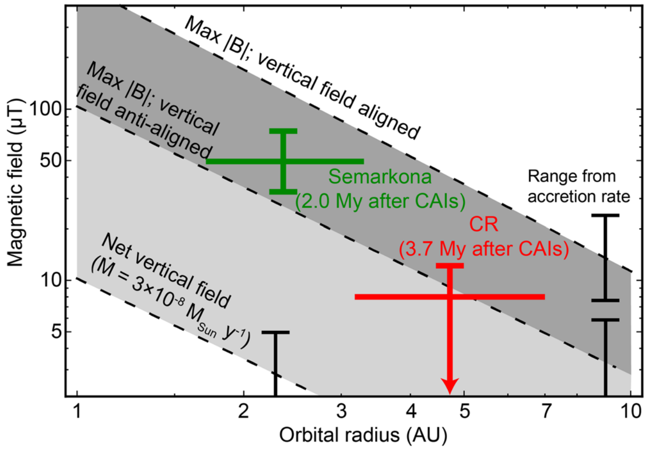

Figure 7. Comparison of magnetic field strengths from MHD disk models and paleomagnetic experiments. Paleointensities of Semarkona and CR chondrules are plotted with 2σ uncertainties and probable formation radii inferred from cosmochemical constraints (see text). The uncertainties plotted for the formation radii are not formal and likely represent nearly the full range of possibilities. Minimum field strength from MHD simulations is the vertical component of the magnetic field assuming transport by disk winds and a solar accretion rate of 3×10^{8} solar masses (M) year^{-1}, which corresponds to a plasma β parameter of 3×10^{4} (Bai, 2015). Depending on the relative orientation of the disk rotation axis and the net vertical field, this net vertical field may be amplified by up to 10–60 times, primarily in the azimuthal direction (Max $|B|$ curves). Due to uncertainty in the solar accretion rate, these maximum field strength estimates are uncertain to approximately a factor of $10^{1/2}$ (black error bars). Local total magnetic field strengths may fluctuate between these maximum values and the minimum set by the net vertical field at <1 AU scales. Modeled magnetic field strengths are computed assuming MMSN conditions. Ages of Semarkona and CR chondrules are based on Kita et al. (2013) and Schrader et al. (2017), respectively.

may not require the presence of gas. The apparent contrast in gas depletion at the angrite and CR formation regions at approximately the same time may be due to earlier removal of gas in the inner solar system, which is the likely formation location of angrites based on isotopic evidence (Sanborn et al., 2019). Alternatively, uncertainties in the ages of CR chondrules and angrites allow the latter to have formed ~0.3 Myr after CR chondrules, permitting a scenario where the dissipation of the nebula occurred in the intervening time.

Therefore, unlike that of the angrites, the paleomagnetic record from CR chondrules reflects magnetic fields in the nebular gas shortly before its dissipation. Chondrule formation models suggest that paleofield intensities recorded in chondrules reflect those of the background nebular magnetic field and not a magnetic field amplified by the chondrule formation mechanism, in both the impact and planetary bow shock scenarios (Fu et al., 2018; Mai et al., 2018). We therefore consider ~8 μT an upper bound on the nebular magnetic field strength at the time and location of CR chondrule formation.

To understand the implications of this constraint on nebular magnetism, we must also estimate the probable formation location of CR chondrules. The higher volatile contents of carbonaceous chondrites point to an origin from ≥3 AU based on the distribution of S- and C-type asteroids in the modern asteroid belt (Demeo & Carry, 2014). Recent evidence from a range of isotopic systems point to the existence of at least two distinct chemical reservoirs in the solar nebula, which may support the idea that carbonaceous chondrites originated beyond the orbit of Jupiter (Kruijer et al., 2017; Van Kooten et al., 2016). If this scenario is correct, then carbonaceous chondrites parent bodies may have originated from a wide range of orbital radii between ~4 and >10 AU (Raymond & Izidoro, 2017; Walsh et al., 2011). However, dust traps leading to distinct chemical reservoirs can potentially be produced by a variety of hypothesized processes that do not require the presence of Jupiter, although further studies are required to confirm the validity of these mechanisms (Dong et al., 2018; Flock et al., 2015; Riols & Lesur, 2019; Suriano et al., 2018). Even if some chondrite groups did form outside the orbit of Jupiter, the apparent similarity between the hydrogen isotopic composition (i.e., the deuterium to hydrogen or D/H ratio) of carbonaceous and ordinary chondrite water suggests a formation within ~7 AU for both groups (Sutton et al., 2017).

The ambient magnetic field strength also depends on the height from the disk midplane. Both the impact and bow shock hypotheses for chondrule formation require the presence of planetesimals and high ambient dust concentration. In the absence of dynamical stirring due to giant planets, the nebular gas rapidly dampens orbital inclinations to <0.3° for Vesta-sized and smaller planetesimals (Kokubo & Ida, 2000), which corresponds to midplane distances of <0.1 scale height in the MMSN. The migration or growth of giant planets may increase planetesimal inclinations to ~2° (Raymond & Izidoro, 2017), corresponding to ~1 scale height displacement from the disk midplane at 5 AU. Regarding the distribution of dust, recent ALMA observations point to efficient vertical settling, likely limiting dust-rich regions capable of chondrule formation via the planetesimal bow shock mechanism to within ~0.1 scale height of the midplane (Boley et al., 2013; Morris et al., 2012; Pinte et al., 2016). Combining these constraints, we conclude that our CR chondrule paleointensity of ≤8 μT applies to the solar nebula between approximately 3 and 7 AU and within ≪1 scale height of the nebula midplane at $3.7^{+0.3}_{-0.2}$ Myr after CAI formation (Figure 7).

We can combine this constraint with the existing estimate of 54 ± 21 μT inferred from Semarkona chondrules, which likely formed between 2 and 3 AU based on the composition of the modern asteroid belt composition and dynamical simulations (Raymond & Izidoro, 2017; Walsh et al., 2011) and ~2.0 Myr after CAIs [full range of single ordinary chondrite ages is 0.7–2.9 Myr with most clustering around 2.0 Myr; (Kita et al., 2013; Mostefaoui et al., 2002; Pape et al., 2019)]. The maximum field intensity of 8.0 ± 4.3 μT we infer from CR chondrites is distinguishable from the 54 ± 21 μT value inferred from Semarkona chondrules at the >4σ level. This contrast is broadly consistent with the weaker magnetic fields expected in the outer solar system assuming a constant rate and mechanism of disk accretion [Figure 7; (Bai, 2015; Fu, Weiss, et al., 2014)].

However, after scaling the paleointensity of Semarkona chondrules to the probable CR formation regions based on the relationship $B \propto R^{-13/8}$ where B is the nebular magnetic field and R is orbital radius [Figure 7; (Bai, 2015)], the nominal magnetic field strength inferred from CR chondrules (≤8 μT) is weaker than the scaled Semarkona value by a factor of ≥2. This low intensity may be explained if CR chondrites formed in the outermost portion of their hypothesized range of origin based on D/H data (i.e., ~7 AU).

Alternatively, the low intensity may be due to temporal variations in nebular magnetic fields. Because the magnetically driven mass accretion rate scales as the square of the magnetic field strength, the weaker ambient magnetic field of CR chondrule formation may imply a greater than or equal to fourfold decay in the disk accretion rate between ~2 and 3.7 Myr after CAI formation. Such a decrease in accretion rates is broadly consistent with observed trends in other protoplanetary disks [e.g.,(Sicilia-Aguilar et al., 2006)], although accretion rates in specific disks can vary by orders of magnitude from the mean trend (Hartmann et al., 1998).

The weak paleointensities recorded by CR chondrules may also be due to spatial variations in the magnetic field strength (Figure 7). Some MHD models have found that vertical magnetic flux may concentrate into ring-like flux sheets that, after reaching steady state, can result in total field strengths that vary by more than 1 order of magnitude on AU length scales (Béthune et al., 2017; Krapp et al., 2018). However, we note that these modeled mechanisms have so far not been observed in stimulations that include all non-ideal MHD effects in a stratified global geometry that resolves disk vertical structure (Riols & Lesur, 2019). Meanwhile, other ring-forming simulations require strong vertical fields that may not be consistent with our CR-derived paleointensities (Béthune et al., 2017; Suriano et al., 2018). As another potential, although less likely, source of spatial heterogeneity, reversals in the direction of the toroidal magnetic field near the midplane, which is required by symmetrical conditions (Bai & Stone, 2013), may create limited zones of weak magnetic fields in chondrule-forming regions (Bai, 2017).

MHD instabilities driving heterogeneities in magnetic field strength, if they exist in real disks, are also projected to cause large-scale fluctuations in dust density (Krapp et al., 2018; Riols & Lesur, 2019). As such, if the weak paleointensities inferred from CR chondrites are due to spatial variations in the magnetic field, they would also provide evidence for the magnetically mediated concentration of gas and dust. In this case, MHD instabilities would be a potential driver of planetesimal formation and the creation of distinct geochemical reservoirs. Further paleomagnetic studies using a range of well-dated samples from both the inner and outer solar system are required to disentangle the effects of temporal and spatial field variations.

Finally, we consider the possibility of using our paleointensity result to constrain the formation region of CR chondrules by comparing the paleointensity to an assumed relationship between the orbital radius and magnetic field intensity. Such a comparison must first assume a mechanism of magnetic angular momentum transport and a polarity of the net vertical magnetic field relative to the solar nebula rotation axis (Figure 7). Even accepting these assumptions, the disk accretion rate in the solar nebula is uncertain by approximately an order of magnitude (black error bars in Figure 7). This last uncertainty alone limits determinations of orbital radius based on magnetic field strength to a factor of ~3. The possibility of heterogeneous MHD enhancements of the toroidal field (see above) introduces further potential uncertainties of a similar magnitude. Finally, uncertainty in the timing of decay for the nebular magnetic field, coupled with uncertainties in the ages of chondrules, further reduce the accuracy of any adopted radius-field strength relationship. As such, paleomagnetic measurements of CR chondrules, similar to other records of instantaneous local field in the solar nebula, can currently only constrain their formation location to an order of magnitude. In the case of CR chondrules, the paleomagnetic data permit their formation anywhere within the 3–7 AU range inferred from compositional data.

5. Conclusion

Our paleomagnetic experiments on 18 chondrule subsamples from two primitive CR chondrites, GRA 95229 and LAP 02342, revealed that the chondrules do not carry any internally unidirectional component of magnetization. Given the meteorites' mild metamorphic history and the primary ferromagnetic mineralogy of the chondrules as verified by electron microscopy and rock magnetic experiments, our results imply that the chondrules did not acquire a coherent remanent magnetization during the cooling in the solar nebula. The expected frequencies of inter-chondrule collisions and the observation of unidirectional magnetization in the chondrules of other meteorites suggest that chondrule tumbling during cooling is unlikely to explain fully the lack of unidirectional magnetization; instead, we conclude that the CR chondrules likely formed in a weak magnetic field below the recording limit of the chondrules' ferromagnetic assemblage.

We used repeated ARM acquisition experiments in progressively weaker bias magnetic fields to quantify the threshold magnetic field value below which the chondrule subsamples can no longer acquire a unidirectional TRM. We accepted a bias field intensity as recordable if the resulting group of ARM directions are statistically non-random and their mean is consistent with the applied bias field direction. Adopting this criterion and correcting for the TRM to ARM ratio for an FeNi ferromagnetic assemblage, we conclude that the CR chondrules likely formed in $a \leq 8$ μT ambient magnetic field.

This upper bound is significantly weaker than the ~50 μT paleointensity inferred from dusty olivine-bearing chondrules from the Semarkona meteorite. The discrepancy may be explained simply by the difference in orbital radii at which the meteorites originated but only if CR chondrites formed near the outer limit of their likely source region inferred from D/H ratios (~7 AU). On the other hand, the weak CR paleointensities may be due to depletion of the nebular gas by $3.7^{+0.3}_{-0.2}$ Myr after CAI formation or spatial heterogeneities in the magnetic field of the solar nebula due to magnetic field self-organization effects. Measurements of nebular field paleointensity from samples of other chondrite groups with a range of ages and source regions are necessary to distinguish these possibilities and to understand the role of magnetic fields in the evolution of the protoplanetary disk and planet formation.

Acknowledgments

We thank A. J. Brearley, A. N. Krot, and B. Zanda for discussions related to sample selection and petrography of the CR chondrites. We also thank K. Righter and C. E. Satterwhite for help sampling the two CR chondrites at the JSC Antarctic meteorites curation facility. We are grateful to J. F. D. F. Araujo and E. A. Lima for help with LAP 02342 data acquisition. Finally, we thank H. Wang and an anonymous reviewer for comments that improved the manuscript. This work was supported by NASA Emerging Worlds Program Grant NNX15AH72G to B. P. W. This work was performed in part at the Harvard Center for Nanoscale Systems (CNS), which is supported by the National Science Foundation under NSF Award 1541959. All demagnetization data reported in this study are available in the MagIC Database under Contribution 16701. All demagnetization data and raw images from the QDM and SQUID microscope are available in the Harvard Dataverse (Fu et al., 2020).

References

ALMA Partnership, Brogan, C., Pérez, L., Hunter, T., Dent, W., Hales, A., Hills, R., et al. (2015). The 2014 ALMA long baseline campaign: First results from high angular resolution observations toward the HL Tau region. *The Astrophysical Journal Letters*, *808*, L3. https://doi.org/10.1088/2041-8205/808/1/L3

Alves, F. O., Girart, J. M., Padovani, M., Galli, D., Franco, G. A. P., Caselli, P., et al. (2018). Magnetic field in a young circumbinary disk. *Astronomy and Astrophysics*, *616*, A56. https://doi.org/10.1051/0004-6361/201832935

Andersson, B.-G., Lazarian, A., & Vaillancourt, J. E. (2015). Interstellar dust grain alignment. *Annual Review of Astronomy and Astrophysics*, *53*, 503–539. https://doi.org/10.1146/annurev-astro-082214-122414

Bai, X.-N. (2015). Hall effect controlled gas dynamics in protoplanetary disks. II. Full 3D simulations toward the outer disk. *The Astrophysical Journal*, *798*, 84. https://doi.org/10.1088/0004-637X/798/2/84

Bai, X.-N. (2017). Global simulations of the inner regions of protoplanetary disks with comprehensive disk microphysics. *The Astrophysical Journal*, *845*(1), 75. https://doi.org/10.3847/1538-4357/aa7dda

Bai, X.-N., & Stone, J. M. (2013). Wind-driven accretion in protoplanetary disks. I. Suppression of the Magnetorotational instability and launching of the magnetocentrifugal wind. *The Astrophysical Journal*, *769*(1), 76. https://doi.org/10.1088/0004-637X/769/1/76

Bai, X.-N., & Stone, J. M. (2017). Hall effect-mediated magnetic flux transport in protoplanetary disks. *The Astrophysical Journal*, *836*(1), 46. https://doi.org/10.3847/1538-4357/836/1/46

Balbus, S. A., & Hawley, J. F. (2000). Solar nebula magnetohydrodynamics. *Space Science Reviews*, *92*(1/2), 39–54. https://doi.org/10.1023/A:1005293132737

Berndt, T., Muxworthy, A. R., & Fabian, K. (2016). Does size matter? Statistical limits of paleomagnetic field reconstruction from small rock specimens. *Journal of Geophysical Research:Solid Earth*, *121*, 15–26. https://doi.org/10.1002/2015JB012441

Béthune, W., Lesur, G., & Ferreira, J. (2017). Global simulations of protoplanetary disks with net magnetic flux I. Non-ideal MHD case. *Astronomy and Astrophysics*, *600*, A75. https://doi.org/10.1051/0004-6361/201630056

Boley, A. C., Morris, M. A., & Desch, S. J. (2013). High-temperature processing of solids through the nebula bow shocks: 3-D radiation hydrodynamics simulations with particles. *The Astrophysical Journal*, *776*, 101. https://doi.org/10.1088/0004-637X/776/2/101

Briani, G., Quirico, E., Gounelle, M., Paulhiac-Pison, M., Montagnac, G., Beck, P., et al. (2013). Short duration thermal metamorphism in CR chondrites. *Geochimica et Cosmochimica Acta*, *122*, 267. https://doi.org/10.1016/j.gca.2013.08.022

Bryson, J. F. J., Neufeld, J. A., & Nimmo, F. (2019). Constraints on asteroid magnetic field evolution and the radii of meteorite parent bodies from thermal modelling. *Earth and Planetary Science Letters*, *521*, 67–78. https://doi.org/10.1016/j.epsl.2019.05.046

Budde, G., Kruijer, T. S., & Kleine, T. (2018). Hf-W chronology of CR chondrites: Implications for the timescales of chondrule formation and the distribution of 26Al in the solar nebula. *Geochimica et Cosmochimica Acta*, *222*, 284–304. https://doi.org/10.1016/j.gca.2017.10.014

Burns, J. A., Lamy, P. L., & Soter, S. (1979). Radiation forces on small particles in the solar system. *Icarus*, *40*, 1–48. https://doi.org/10.1016/0019-1035(79)90050-2

Carporzen, L., Weiss, B. P., Elkins-Tanton, L. T., Shuster, D. L., Ebel, D. S., & Gattacceca, J. (2011). Magnetic evidence for a partially differentiated carbonaceous chondrite parent body. *Proceedings of the National Academy of Sciences of the United States of America*, *108*, 6386–6389. https://doi.org/10.1073/pnas.1017165108

Carrera, D., Johansen, A., & Davies, M. B. (2015). How to form planetesimals from mm-sized chondrules and chondrule aggregates. *Astronomy and Astrophysics*, *579*, A43. https://doi.org/10.1051/0004-6361/201425120

Chambers, J. E. (2010). Planetesimal formation by turbulent concentration. *Icarus*, *208*, 505–517. https://doi.org/10.1016/j.icarus.2010.03.004

Cournede, C., Gattacceca, J., Gounelle, M., Rochette, P., Weiss, B. P., & Zanda, B. (2015). An early solar system magnetic field recorded in CM chondrites. *Earth and Planetary Science Letters*, *410*, 62–74. https://doi.org/10.1016/j.epsl.2014.11.019

Crutcher, R. M. (2012). Magnetic fields in molecular clouds. *Annual Review of Astronomy and Astrophysics*, *50*, 29–53. https://doi.org/10.1146/annurev-astro-081811-125514

Davidson, J., Schrader, D. L., Alexander, C. M. O., Nittler, L. R., & Bowden, R. (2019). Re-examining thermal metamorphism of the Renazzo-like (CR) carbonaceous chondrites: Insights from pristine Miller Range 090657 and shock-heated Graves Nunataks 06100. *Geochimica et Cosmochimica Acta*, *267*, 240–256. https://doi.org/10.1016/j.gca.2019.09.033

Demeo, F. E., & Carry, B. (2014). Solar system evolution from compositional mapping of the asteroid belt. *Nature*, *505*(7485), 629–634. https://doi.org/10.1038/nature12908

de Pater, I., & Lissauer, J. J. (2010). *Dissipative forces and the orbits of small bodies, in: Planetary sciences*, (pp. 45–49). New York: Cambridge University Press.

Dong, R., Li, S., Chiang, E., & Li, H. (2018). Multiple disk gaps and rings generated by a single super-Earth. II. Spacings, depths, and number of gaps, with application to real systems. *The Astrophysical Journal*, *866*, 110. https://doi.org/10.3847/1538-4357/aadadd

Flock, M., Ruge, J. P., Dzyurkevich, N., Henning, T., Klahr, H., & Wolf, S. (2015). Gaps, rings, and non-axisymmetric structures in protoplanetary disks. *Astronomy and Astrophysics*, *574*, A68. https://doi.org/10.1051/0004-6361/201424693

Fu, R. R., Kehayias, P., Weiss, B. P., Schrader, D. L., Bai, X. -N., & Simon, J. B. (2020). Replication data for: Weak magnetic fields in the outer solar nebula recorded in CR chondrites, Harvard Dataverse, V1, doi:10.7910/DVN/FBSJLL.

Fu, R. R., Lima, E. A., & Weiss, B. P. (2014). No nebular magnetization in the Allende CV carbonaceous chondrite. *Earth and Planetary Science Letters*, *404*, 54–66. https://doi.org/10.1016/j.epsl.2014.07.014

Fu, R. R., & Weiss, B. P. (2012). Detrital remanent magnetization in the solar nebula. *Journal of Geophysical Research*, *117*, E02003. https://doi.org/10.1029/2011JE003925

Fu, R. R., Weiss, B. P., Lima, E. A., Harrison, R. J., Bai, X.-N., Desch, S. J., et al. (2014). Solar nebula magnetic fields recorded in the Semarkona meteorite. *Science*, *346*(6213), 1089–1092. https://doi.org/10.1126/science.1258022

Fu, R. R., Weiss, B. P., Lima, E. A., Kehayias, P., Araujo, J. F. D. F., Glenn, D. R., et al. (2017). Evaluating the paleomagnetic potential of single zircon crystals using the Bishop Tuff. *Earth and Planetary Science Letters*, *458*, 1–13. https://doi.org/10.1016/j.epsl.2016.09.038

Fu, R. R., Weiss, B. P., Schrader, D. L., & Johnson, B. C. (2018). Records of magnetic fields in the chondrule formation environment. In *Chondrules* (pp. 324–340). Cambridge U.K.: Cambridge University press.

Gammie, C. F. (1996). Layered accretion in T Tauri disks. *The Astrophysical Journal*, *457*, 355–362. https://doi.org/10.1086/176735

Garvie, L. A. J., Knauth, L. P., & Morris, M. A. (2017). Sedimentary laminations in the Isheyevo (CH/CBb) carbonaceous chondrite formed by gentle impact-plume sweep-up. *Icarus*, *292*, 36–47. https://doi.org/10.1016/j.icarus.2017.03.021

Gattacceca, J., Rochette, P., & Bourot-Denise, M. (2003). Magnetic properties of a freshly fallen LL ordinary chondrite: The Bensour meteorite. *Physics of the Earth and Planetary Interiors*, *140*, 343–358. https://doi.org/10.1016/j.pepi.2003.10.001

Glenn, D. R., Fu, R. R., Kehayias, P., Le Sage, D., Lima, E. A., Weiss, B. P., & Walsworth, R. L. (2017). Micrometer-scale magnetic imaging of geological samples using a quantum diamond microscope. *Geochemistry, Geophysics, Geosystems*, *18*, 3254–3267. https://doi.org/10.1002/2017GC006946

Hartmann, L., Calvet, N., Gullbring, E., & D'Alessio, P. (1998). Accretion and the evolution of T Tauri stars. *The Astrophysical Journal*, *495*, 385–400. https://doi.org/10.1086/305277

Hoffman, K. A., Baker, J. R., & Banerjee, S. K. (1979). Combining paleointensity methods: A dual-valued determination on lunar sample 10017,135. *Physics of the Earth and Planetary Interiors*, *20*, 317–323. https://doi.org/10.1016/0031-9201(79)90054-2

Horng, C.-S., & Roberts, A. P. (2018). The low-temperature Besnus magnetic transition: Signals due to monoclinic and hexagonal pyrrhotite. *Geochemistry, Geophysics, Geosystems*, *19*, 3364–3375. https://doi.org/10.1029/2017GC007394

Hu, X., Zhu, Z., Okuzumi, S., Bai, X.-N., Wang, L., Tomida, K., & Stone, J. M. (2019). Non-ideal MHD simulation of HL Tau disk: Formation of rings. *The Astrophysical Journal*, *885*, 36. https://doi.org/10.3847/1538-4357/ab44cb

Isella, A., Guidi, G., Testi, L., Liu, S., Li, H., Li, S., et al. (2016). Ringed structures of the HD 163296 protoplanetary disk revealed by ALMA. *Physical Review Letters*, *117*, 251101. https://doi.org/10.1103/physrevlett.117.251101s

Johansen, A., Mac Low, M.-M., Lacerda, P., & Bizzarro, M. (2015). Growth of asteroids, planetary embryos, and Kuiper belt objects by chondrule accretion. *Science Advances*, *1*, e1500109. https://doi.org/10.1126/sciadv.1500109

Johansen, A., Oishi, J. S., Mac Low, M.-M., Klahr, H., Henning, T., & Youdin, A. (2007). Rapid planetesimal formation in turbulent circumstellar disks. *Nature*, *448*(7157), 1022–1025. https://doi.org/10.1038/nature06086

Johnson, B. C., Minton, D. A., Melosh, H. J., & Zuber, M. T. (2015). Impact jetting as the origin of chondrules. *Nature*, *517*(7534), 339–341. https://doi.org/10.1038/nature14105

Kataoka, A., Muto, T., Momose, M., Tsukagoshi, T., Fukagawa, M., Shibai, H., et al. (2015). Millimeter-wave polarization of protoplanetary disks due to dust scatterting. *The Astrophysical Journal*, *809*, 78. https://doi.org/10.1088/0004-637X/809/1/78

Kimura, H., Okamoto, H., & Mukai, T. (2002). Radiation pressure and the Poynting–Robertson effect for fluffy dust particles. *Icarus*, *157*, 349–361. https://doi.org/10.1006/icar.2002.6849

Kirschvink, J. L. (1980). The least-squares line and plane and the analysis of paleomagnetic data: Examples from Siberia and Morocco. *Geophysical Journal of the Royal Astronomical Society*, *62*, 699–718.

Kita, N. T., Yin, Q.-Z., MacPherson, G. J., Ushikubo, T., Jacobsen, B., Nagashima, K., et al. (2013). ^{26}Al-^{26}Mg isotope systematics of the first solids in the early solar system. *Meteoritics and Planetary Science*, 1–18. https://doi.org/10.1111/maps.12141

Klahr, H., Pfeil, T., & Schreiber, A. (2018). Instabilities and flow structures in protoplanetary disks: Setting the stage for planetesimal formation. In *Handbook of Exoplanets*, (pp. 1–39). Cham, Switzerland: Springer.

Kokubo, E., & Ida, S. (2000). Formation of protoplanets from planetesimals in the solar nebula. *Icarus*, *143*, 15–27. https://doi.org/10.1006/icar.1999.6237

Krapp, L., Gressel, O., Benítez-Llambay, P., Downes, T. P., Mohandas, G., & Pessah, M. E. (2018). Dust segregation in Hall-dominated turbulent protoplanetary disks. *The Astrophysical Journal*, *865*, 105. https://doi.org/10.3847/1538-4357/aadcf0

Kruijer, T. S., Burkhardt, G., Budde, G., & Kleine, T. (2017). Age of Jupiter inferred from the distinct genetics and formation times of meteorites. *Proceedings of the National Academy of Sciences of the United States of America*, *14*, 6712.

Kunz, M. W. (2008). On the linear stability of weakly ionized, magnetized planar shear flows. *Monthly Notices of the Royal Astronomical Society*, *385*, 1494–1510. https://doi.org/10.1111/j.1365-2966.2008.12928.x

Kunz, M. W., & Lesur, G. (2013). Magnetic self-organization in Hall-dominated magnetorotational turbulence. *Monthly Notices of the Royal Astronomical Society*, *434*, 2295–2312. https://doi.org/10.1093/mnras/stt1171
Lappe, S.-C. L. L., Harrison, R. J., Feinberg, J. M., & Muxworthy, A. (2013). Comparison and calibration of nonheating paleointensity methods: A case study using dusty olivine. *Geochemistry, Geophysics, Geosystems*, *14*, 2143–2158. https://doi.org/10.1002/ggge.20141
Lesur, G., Kunz, M. W., & Fromang, S. (2014). Thanatology in protoplanetary discs: The combined influence of Ohmic, Hall, and ambipolar diffusion on dead zones. *Astronomy and Astrophysics*, *566*, A56. https://doi.org/10.1051/0004-6361/201423660
Li, D., Pantin, E., Telesco, C. M., Zhang, H., Wright, C. M., Barnes, P. J., et al. (2016). An ordered magnetic field in the protoplanetary disk of AB Aur revealed by mid-infrared polarimetry. *The Astrophysical Journal*, *832*, 18. https://doi.org/10.3847/0004-637X/832/1/18
Lima, E. A., & Weiss, B. P. (2009). Obtaining vector magnetic field maps from single-component measurements of geological samples. *Journal of Geophysical Research*, *114*, B06102. https://doi.org/10.1029/2008JB006006
Lima, E. A., & Weiss, B. P. (2016). Ultra-high sensitivity moment magnetometry of geological samples using magnetic microscopy. *Geochemistry, Geophysics, Geosystems*, *17*, 3754–3774. https://doi.org/10.1002/2016GC006487
Lowrie, W. (1990). Identification of ferromagnetc minerals in a rock by coercivity and unblocking temperature properties. *Geophysical Research Letters*, *17*, 159–162. https://doi.org/10.1029/GL017i002p00159
Mai, C., Desch, S. J., Boley, A. C., & Weiss, B. P. (2018). Magnetic fields recorded by chondrules formed in nebular shocks. *The Astrophysical Journal*, *857*, 96. https://doi.org/10.3847/1538-4357/aab711
Morden, S. J. (1992). A magnetic study of the Millbillillie (eucrite) achondrite: Evidence for dynamo-type magnetising field. *Meteoritics*, *27*, 560–567. https://doi.org/10.1111/j.1945-5100.1992.tb01077.x
Morris, M. A., Boley, A. C., Desch, S. J., & Athanassiadou, T. (2012). Chondrule formation in bow shocks around eccentric planetary embryos. *The Astrophysical Journal*, *752*, 27. https://doi.org/10.1088/0004-637X/752/1/27
Mostefaoui, S., Kita, N. T., Togashi, S., Tachibana, S., Nagahara, H., & Morishita, Y. (2002). The relative num-26/aluminum-27 ratios. *Meteoritics and Planetary Science*, *37*, 421–438. https://doi.org/10.1111/j.1945-5100.2002.tb00825.x
Nagata, T. (1979a). Meteorite magnetism and the early solar system magnetic field. *Physics of the Earth and Planetary Interiors*, *20*, 324–341.
Nagata, T. (1979b). Magnetic properties and paleointensity of achondrites in comparison with those of lunar rocks. Proc Lunar Planet Sci Conf 10th 2199–2210.
Ohashi, S., Kataoka, A., Nagai, H., Momose, M., Muto, T., Hanawa, T., et al. (2018). Two different grain size distributions within the protoplanetary disk around HD 142527 revealed by ALMA polarization observation. *The Astrophysical Journal*, *864*, 81. https://doi.org/10.3847/1538-4357/aad632
Pape, J., Mezger, K., Bouvier, A.-S., & Baumgartner, L. P. (2019). Time and duration of chondrule formation: Constraints from ^{26}Al-^{26}Mg ages of individual chondrules. *Geochimica et Cosmochimica Acta*, *244*, 416–436. https://doi.org/10.1016/j.gca.2018.10.017
Pinte, C., Dent, W. R. F., Ménard, F., Hales, A., Hill, T., Cortes, P., & de Gregorio-Monsalvo, I. (2016). Dust and gas in the disk of HL Tauri: Surface density, dust settling, and dust-to-gas ratio. *The Astrophysical Journal*, *816*, 25. https://doi.org/10.3847/0004-637x/816/1/25
Raymond, S. N., & Izidoro, A. (2017). Origin of water in the inner solar system: Planetesimals scattered inward during Jupiter and Saturn's rapid gas accretion. *Icarus*, *297*, 134–148. https://doi.org/10.1016/j.icarus.2017.06.030
Reisener, R. J., & Goldstein, J. I. (2003). Ordinary chondrite metallography: Part 1. Fe-Ni taenite cooling experiments. *Meteoritics and Planetary Science*, *38*, 1669–1678. https://doi.org/10.1111/j.1945-5100.2003.tb00007.x
Riols, A., & Lesur, G. (2019). Spontaneous ring formation in wind-emitting accretion discs. *Astronomy and Astrophysics*, *625*, A108. https://doi.org/10.1051/0004-6361/201834813
Ryan, B. R., Gammie, C. F., Fromang, S., & Kestener, P. (2017). Resolution dependence of magnetorotational turbulence in the isothermal stratified shearing box. *The Astrophysical Journal*, *840*, 6. https://doi.org/10.3847/1538-4357/aa6a52
Sanborn, M. E., Wimpenny, J., Williams, C. D., Yamakawa, A., Amelin, Y., Irving, A. J., & Yin, Q.-Z. (2019). Carbonaceous achondrites Northwest Africa 6704/6693: Milestones for early solar system chronology and genealogy. *Geochimica et Cosmochimica Acta*, *245*, 577–596. https://doi.org/10.1016/j.gca.2018.10.004
Schrader, D. L., Connolly, H. C., Lauretta, D. S., Zega, T. J., Davidson, J., & Domanik, K. J. (2015). The formation and alteration of the Renazzo-like carbonaceous chondrites III: Toward understanding the genesis of ferromagnesian chondrules. *Meteoritics and Planetary Science*, *50*, 15–50. https://doi.org/10.1111/maps.12402
Schrader, D. L., Davidson, J., & McCoy, T. J. (2016). Widespread evidence for high-temperature formation of pentlandite in chondrites. *Geochimica et Cosmochimica Acta*, *189*, 359–376. https://doi.org/10.1016/j.gca.2016.06.012
Schrader, D. L., Fu, R. R., Desch, S. J., & Davidson, J. (2018). The background temperature of the protoplanetary disk within the first four million years of the solar system. *Earth and Planetary Science Letters*, *504*, 30. https://doi.org/10.1016/j.epsl.2018.09.030
Schrader, D. L., & Lauretta, D. S. (2010). High-temperature experimental analogs of primitive meteoritic metal–sulfide–oxide assemblages. *Geochimica et Cosmochimica Acta*, *74*, 1719–1733. https://doi.org/10.1016/j.gca.2009.11.030
Schrader, D. L., Nagashima, K., Krot, A. N., Ogliore, R. C., Yin, Q. Z., Amelin, Y., et al. (2017). Distribution of ^{26}Al in the CR chondrite chondrule-forming region of the protoplanetary disk. *Geochimica et Cosmochimica Acta*, *201*, 275–302. https://doi.org/10.1016/j.gca.2016.06.023
Schrader, D. L., Nagashima, K., Waitukaitis, S. R., Davidson, J., McCoy, T. J., Connolly, H. C., & Lauretta, D. S. (2018). The retention of dust in protoplanetary disks: Evidence from agglomeratic olivine chondrules from the outer solar system. *Geochimica et Cosmochimica Acta*, *223*, 405–421. https://doi.org/10.1016/j.gca.2017.12.014
Shu, F. H., Shang, H., & Lee, T. (1996). Toward an astrophysical theory of chondrites. *Science*, *271*, 1545–1552. https://doi.org/10.1126/science.271.5255.1545
Sicilia-Aguilar, A., Hartmann, L., Calvet, N., Megeath, S. T., Muzerolle, J., Allen, L., et al. (2006). Disk evolution in Cep OB2: Results from the Spitzer space telescope. *The Astrophysical Journal*, *638*, 897–919. https://doi.org/10.1086/498085
Simon, J. B., Bai, X.-N., Armitage, P., Stone, J. M., & Beckwith, K. (2013). Turbulence in the outer regions of protoplanetary disks. II. Strong accretion driven by a vertical magnetic field. *The Astrophysical Journal*, *775*(1), 73. https://doi.org/10.1088/0004-637X/775/1/73
Simon, J. B., Bai, X.-N., Flaherty, K. M., & Hughes, A. M. (2018). Origin of weak turbulence in the outer regions of protoplanetary disks. *The Astrophysical Journal*, *865*, 10. https://doi.org/10.3847/1538-4357/aad86d
Simon, J. B., Bai, X.-N., Stone, J. M., Armitage, P., & Beckwith, K. (2013). Turbulence in the outer regions of protoplanetary disks. I. Weak accretion with no vertical magnetic flux. *The Astrophysical Journal*, *764*(1), 66. https://doi.org/10.1088/0004-637X/764/1/66
Simon, J. B., Lesur, G., Kunz, M. W., & Armitage, P. J. (2015). Magnetically driven accretion in protoplanetary discs. *Monthly Notices of the Royal Astronomical Society*, *454*, 1117. https://doi.org/10.1093/mnras/stv2070
Singerling, S. A., & Brearley, A. J. (2018). Primary iron sulfides in CM and CR carbonaceous chondrites: Insights into nebular processes. *Meteoritics and Planetary Science*, *53*, 2078–2106. https://doi.org/10.1111/maps.13108

Stephens, I. W., Looney, L. W., Kwon, W., Fernández-López, M., Hughes, A. M., Mundy, L. G., et al. (2014). Spatially resolved magnetic field structure in the disk of a T Tauri star. *Nature*, *514*(7524), 597–599. https://doi.org/10.1038/nature13850

Stephens, I. W., Yang, H., Li, Z.-Y., Looney, L. W., Kataoka, A., Kwon, W., et al. (2017). ALMA reveals transition of polarization pattern with wavelength in HL Tau's disk. *The Astrophysical Journal*, *851*, 55. https://doi.org/10.3847/1538-4357/aa998b

Stephenson, A. (1993). Three-axis alternating field demagnetization of rocks and the identification of natural remanent magnetization, gyromagnetic magnetization, and anisotropy. *Journal of Geophysical Research*, *98*, 373–381. https://doi.org/10.1029/92JB01849

Stephenson, A., & Collinson, D. W. (1974). Lunar magnetic field palaeointensities determined by an anhysteretic remanent magnetization method. *Earth and Planetary Science Letters*, *23*, 220–228. https://doi.org/10.1016/0012-821X(74)90196-4

Stephenson, A., Collinson, D. W., & Runcorn, S. K. (1976). On the intensity of the ancient lunar magnetic field. Proc Lunar Sci Conf 7th 3373–3382, DOI: 10.1007/BF01570250.

Suavet, C., Weiss, B. P., & Grove, T. L. (2014). Controlled-atmosphere thermal demagnetization and paleointensity analyses of extraterrestrial rocks. *Geochemistry, Geophysics, Geosystems*, *15*, 2733–2743. https://doi.org/10.1002/2013GC005215

Suriano, S. S., Li, Z.-Y., Krasnopolsky, R., & Shang, H. (2018). The formation of rings and gaps in magnetically coupled disc-wind systems: Ambipolar diffusion and reconnection. *Monthly Notices of the Royal Astronomical Society*, *477*(1), 1239–1257. https://doi.org/10.1093/mnras/sty717

Sutton, S., Alexander, C. M. O., Bryant, A., Lanzirotti, A., Newville, M., & Cloutis, E. A. (2017). The bulk valence state of Fe and the origin of water in chondrites. *Geochimica et Cosmochimica Acta*, *211*, 115. https://doi.org/10.1016/j.gca.2017.05.021

Swartzendruber, L. J., Itkin, V. P., & Alcock, C. B. (1991). The Fe-Ni (iron-nickel) system. *Journal of Phase Equilibria*, *12*, 288–312. https://doi.org/10.1007/BF02649918

Tikoo, S. M., Weiss, B. P., Buz, J., Lima, E. A., Shea, E. K., Melo, G., & Grove, T. L. (2012). Magnetic fidelity of lunar samples and implications for an ancient core dynamo. *Earth and Planetary Science Letters*, *337–338*, 93–103. https://doi.org/10.1016/j.epsl.2012.05.024

Van Kooten, E. M. M. E., Wielandt, D., Schiller, M., Nagashima, K., Thomen, A., Larsen, K. K., et al. (2016). Isotopic evidence for primordial molecular cloud material in metal-rich carbonaceous chondrites. *Proceedings of the National Academy of Sciences of the United States of America*, *113*(8), 2011–2016. https://doi.org/10.1073/pnas.1518183113

Vlemmings, W. H. T., Lankhaar, B., Cazzoletti, P., Ceccobello, C., Dall'Olio, D., van Dishoeck, E. F., et al. (2019). Stringent limits on the magnetic field strength in the disc of TW Hya ALMA observations of CN polarisation. *Astronomy and Astrophysics*, *624*, L7. https://doi.org/10.1051/0004-6361/201935459

Walsh, K. J., Morbidelli, A., Raymond, S. N., O'Brien, D. P., & Mandell, A. M. (2011). A low mass for Mars from Jupiter's early gas-driven migration. *Nature*, *475*(7355), 206–209. https://doi.org/10.1038/nature10201

Wang, H., Weiss, B. P., Bai, X.-N., Downey, B. G., Wang, J., Wang, J., et al. (2017). Lifetime of the solar nebula constrained by meteorite paleomagnetism. *Science*, *355*(6325), 623–627. https://doi.org/10.1126/science.aaf5043

Wasilewski, P. (1981). Magnetization of small iron-nickel spheres. *Physics of the Earth and Planetary Interiors*, *26*, 149–161. https://doi.org/10.1016/0031-9201(81)90106-0

Watson, G. S. (1956). Analysis of dispersion on a sphere. *Monthly Notices of the Royal Astronomical Society*, *7*, 153–159. https://doi.org/10.1111/j.1365-246X.1956.tb05560.x

Weiss, B. P., & Tikoo, S. M. (2014). The lunar dynamo. *Science*, *346*, 1,246,753–1,246,753. https://doi.org/10.1126/science.1246753

Wick, M. J., & Jones, R. H. (2012). Formation conditions of plagioclase-bearing type I chondrules in CO chondrites: A study of natural samples and experimental analogs. *Geochimica et Cosmochimica Acta*, *98*, 140–159. https://doi.org/10.1016/j.gca.2012.09.027

Yang, C.-W., Williams, D. B., & Goldstein, J. I. (1997). Low-temperature phase decomposition in metal from iron, stony-iron, and stony meteorites. *Geochimica et Cosmochimica Acta*, *61*, 2943–2956. https://doi.org/10.1016/S0016-7037(97)00132-4

Zhu, Z., & Stone, J. M. (2014). Dust trapping by vortices in transitional disks: Evidence for non-ideal magnetohydrodynamic effects in protoplanetary disks. *The Astrophysical Journal*, *795*, 53. https://doi.org/10.1088/0004-637X/795/1/53

Zsom, A., Ormel, C. W., Güttler, C., Blum, J., & Dullemond, C. P. (2010). The outcome of protoplanetary dust growth: Pebbles, boulders, or planetesimals? *Astronomy and Astrophysics*, *513*, A57. https://doi.org/10.1051/0004-6361/200912976